An Ogden-like formulation incorporating phase-field fracture in elastomers: From brittle to pseudo-ductile failures

note finali coverpage

(Article begins on next page)

25 August 2024

An Ogden-like formulation incorporating phase-field fracture in elastomers: from brittle to pseudo-ductile failures

Jacopo Ciambella[1], Giovanni Lancioni[2], and Nico Stortini[3]

[1]Department of Structural and Geotechnical Engineering, Sapienza University of Rome, Rome, Italy.
[2]Department of Civil and Building Engineering and Architecture, Polytechnic University of Marche, Ancona, Italy.
[3]Department of Mechanics and Aeronautics, Sapienza University of Rome, Rome, Italy.

March 8, 2022

Abstract

Over the past 50 years Ogden model has been widely used in material modelling due to its ability to match accurately the experimental data on elastomers at large strain, as well as for its mathematical properties, such as polyconvexity. In this paper these peculiarities are exploited to formulate a three-dimensional finite strain model that incorporates, through a phase-field approach, a cohesive damage mechanism which leads to the progressive degradation of the material stiffness and to failure under tension. The model is calibrated by using data on double-network elastomers which display a pseudo-ductile damage behaviour at large strain. However the formulation is presented in a general framework and it is shown that by properly tailoring the constitutive parameters it is possible to encompass a wide range of effects from brittle to pseudo-ductile failure processes. As such the proposed model is applicable to describe fracture coalescence and propagation in a wide range of materials.

Kyeywords: Large strain, phase-field fracture, hyperelasticity, elastomer

1

1 Introduction

Over the past 50 years the phenomenological hyperelastic model proposed by Ogden for compressibile [1] and incompressibile [2] elastomers has been successfully adopted for a variety of materials including rubber [3, 4, 5, 6], nematic elastomers [7, 8], foams [9, 10], biological tissues [11, 12, 13] and even for carbon nanotubes [14]. The main feature of the Ogden model is that it postulates a form of the strain energy density in terms of the principal stretches rather than the classical strain invariants as the majority of hyperelastic models do. The principal stretches make the closed form expression of the tangent moduli easily calculable [3] and so the model is easily implementable in finite element algorithms. The model has also a strong mathematical basis as it satisfies policonvexity.

The strain energy density of the Ogden model is written as the sum of three separate functions of the principal stretches λ_1, λ_2 and λ_3:

$$\phi(\lambda_1, \lambda_2, \lambda_3) = \sum_{a=1}^{3} \tilde{\phi}(\lambda_a), \qquad \text{with} \quad \tilde{\phi}(\lambda_a) = \sum_{n=1}^{N} \frac{\mu_n}{\alpha_n} (\lambda_a^{\alpha_n} - 1), \quad (1)$$

making it adherent to the so-called Valanis–Landel split [15]. Each term $\tilde{\phi}(\lambda_a)$ in the series (1) represents the elastic energy of a nonlinear spring undergoing a stretch λ_a; the corresponding stiffness $\mu_n \alpha_n$ can be tailored to describe all aspects of the rubber elastic response, starting from the initial softening for moderate strains, to the stress hardening at large strains. For most quasi-static experiments on rubber, three terms in the series give an excellent correlation with stress-strain data [16].

All these remarkable properties are exploited to formulate a phenomenological theory for the cohesive failure of elastomeric materials at large strain. The model incorporates, through a phase-field approach, the mechanisms which lead to the softening behaviour and to the progressive degradation of the material stiffness at large strain.

The phase-field approach that we follow relies on the variational theory of fracture mechanics introduced in [17], where the fracture problem for brittle elastic bodies was formulated as a free-discontinuity minimum problem. The variational formulation of fracture was approximated in [18] by a regularized problem that operates on a functional defined on continuous fields, with fracture replaced by the so-called *phase-field* variable. Acting like a damage variable, the phase-field assumes values between 0 and 1, with 0 for sound material and 1 for the fractured material, and its evolution describes the coalescence and propagation of cracks [19, 20, 21]. As the phase-field

2

increases, the stiffness of the material reduces, vanishing when the damage variable reaches 1. A non-local term, proportional to the gradient of the phase-field, is also incorporated into the internal energy functional and it plays the role of localization limiter by penalizing abrupt damage variations [22], and by promoting smooth transitions from 0 to 1 in regions of finite width. The gradient contribution automatically introduces an internal length, that in the present formulation is a constitutive parameter, to be calibrated through experimental data [23], and it makes the model size dependent. Smoothness properties of phase-field approaches allow for straightforward standard finite elements implementation, and no remeshing or ad-hoc numerical strategies need to be used, making the solution of the numerical problem robust and independent of the mesh used in the finite element simulations.

Many contributions are available in the literature concerning phase-field formulations for brittle materials undergoing large deformations. A first model was proposed in [24], where phase-field fracture was incorporated within the framework of finite elasticity in order to improve the description of stretching near crack tips, where large strains usually develop. Following a phase-field approach, a rate-independent model was formulated in [22] to model the fracture in elastomers, and it was extended in [25] by including viscous effects. A multiplicative splitting of the stretch into tensile and compressive parts was proposed in [26] to describe fracture mechanisms induced by tensile stress states. Cavitation processes in elastomers, with voids coalescing and developing into fractures, were reproduced in [27] by using a specific nonlinear polyconvex strain energy. A phase-field model for the description of cavitation was also proposed in [28] and improved in [29], and is based on three features, according to the experimental evidence of [30, 31]: *i.* a criterion of fracture nucleation driven by hydrostatic stress, *ii.* the possibility of fracture healing, and *iii.* a dependence of the material resistance on the cumulative history of fracture and healing. A bottom-up multi-scale approach was followed in [32]. It was assumed that the internal energy at the micro-scale is composed by an entropic contribution due to the polymer chains configurational entropy, and an energetic contribution due to bond deformation, such that the latter contribution drives crack nucleation, initiation and propagation. Then, bridging the microscopic assumptions to the macro-scale, a continuum model was obtained where fracture was approximated by a phase field. A phase-field model was also proposed in [33] based on the micro-mechanics of polydisperse elastomer networks, that is, distributions of polymeric chains with different lengths.

Although elastomers are capable of sustaining large deformations, how-

ever their failure is brittle, and this may greatly limit their application in the fields of automotive, structural, biomedical engineering, etc.. Nowadays, great efforts are devoted to the development of new elastomeric composite with enhanced mechanical properties, such as strength, ductility, and durability. Increased ductility is often combined with processes of progressive material damaging that gradually leads to fracture, as in quasi-brittle or cohesive fracture. These failure modes were observed in elastomeric composites such as highly filled elastomers, in which the mechanism of cohesive failure is activated at the filler-matrix interface [34], or double-network elastomers, which have been recently synthesized in [35]. This rubber material, compared to traditional elastomers, has a *double network* internal structure constituted by a stretchy elastomeric matrix reinforced with a continuous filler network, that confers to the composite unique mechanical properties. Conventional single network elastomers are able to bear large deformations thanks to their intertwined spaghetti-like internal structure. However an important limitation is that a local defect, such as a chain rupture or a void, quickly propagates and may lead to the catastrophic failure of the whole specimen [36]. On the other hand, the presence of the additional filler network leads to a strong localized softening, due to rupture of covalent bonds and coalescence of defects, followed by a stable necking process. The micro defects propagate only when the energy release rate of defect cavitation exceeds the intrinsic fracture toughness of the matrix. The resulting macroscopic behaviour shows a ductile-like curve at large strain obtained when the load can be efficiently transferred from the filler network to the matrix network [37].

Therefore we aim at introducing a phase-field model capable of describing a variety of different failure processes at large strains, from brittle to pseudo-ductile. In doing so we use the framework introduced in [38], where a phase-field theory incorporating constitutive functions for both brittle and quasi-brittle fracture was formulated within the context of infinitesimal elasticity. The advantages of this theory is that the softening laws frequently adopted for quasi-brittle solids, e.g., linear, exponential and hyperbolic ones, etc., are easily reproduced. In addition the constitutive functions of the fracture energy converges to a cohesive zone model as the internal length scale vanishes [38]. We therefore formulate our model in a general framework, such that those popular phase-field models for brittle fracture, e.g., [20], [21], etc., can be recovered as the particular examples. The optimal constitutive parameters of the model are calibrated by studying the one-dimensional problem of a bar under traction, that allows us to solve the problem in semi-analytical form.

The paper is organised as follows. Section 2 is devoted to the formulation of the three-dimensional model in a consistent thermodynamic framework. It addresses the theoretical aspect of the proposed phase-field theory. Section 3 is devoted to the calibration of the model parameter by solving the one-dimensional problem of a bar under traction. The numerical solutions of some prototypical examples are presented and discussed in Section 4, including a through comparison of the model prediction with the experimental data in [35]. Concluding remarks are drawn in Section 5.

2 Model formulation

In this Section we aim at formulating the nonlinear elastic model with damage in a general three-dimensional settings, before carrying out in Sec. 3 a sensitivity analysis by considering the response of a bar under traction. The approach adopted to equilibrium is based on a unilateral minimality principle under the condition of irreversibility of the damage field. The same approach has been widely adopted in plasticity [39, 24, 40], plasticity with damage [41, 42] and cohesive damage [38, 43].

Throughout the paper we will assume that all fields are sufficiently smooth so that all the calculations can be performed. For a precise definition of the functional spaces needed the reader is referred to [44].

A note on the notation. In the following small bold letters will be used for points or vectors, whereas capital bold letters for tensors. The inner product between two vectors or two tensors of the same order will be indicated by a dot, such as $\mathbf{a} \cdot \mathbf{b} = \sum_i a_i b_i$ or $\mathbf{A} \cdot \mathbf{B} = \sum_{i,j} A_{ij} B_{ij}$. An overdot will indicate the material time derivative, whereas a prime will indicate the derivative with respect to the independent variable, e.g., the position x or the variable d.

2.1 State variables

We identify a body with a region Ω_0 of the three-dimensional Euclidean space $\mathcal{E}$, that occupies at some time instant $t = 0$, which we denote as the *reference configuration*. The external boundary $\partial\Omega_0$ is divided into a subset $\partial\Omega_0^u$ in which displacement is applied, and a complementary boundary $\partial\Omega_0^t$ in which surface forces are present. The deformation of the body is the bijective orientation-preserving map $p : \Omega_0 \times [0, t] \to \mathcal{E}$ which assigns at each point $\mathbf{x} \in \Omega_0$ a point $\mathbf{y} = p(\mathbf{x}, t)$ in the deformed configuration; accordingly we set $\Omega_t = p(\Omega_0, t)$ as the deformed configuration of the body.

At each material point $\mathbf{x}$, the state of the continuum is identified by the displacement field $\mathbf{u}(\mathbf{x}, t)$ and by an additional scalar field $d(\mathbf{x}, t)$, that represents the *damage variable*, such that $d = 0$ for the virgin material and $d = 1$ for the fully damaged one; in this formulation, d is a Lagrangean parameter defined on the reference configuration Ω_0. We further denote by $\mathscr{U}$ the space of kinematically admissible displacement field

$$\mathbf{u}(\mathbf{x}, t) \in \mathscr{U} := \{\mathbf{u} : \mathbf{u}(\mathbf{x}, t) = \mathbf{u}^* \ \forall \mathbf{x} \in \partial\Omega_0^u\},$$

and with $\mathscr{D}$ the set of the admissible damage field

$$d(\mathbf{x}, t) \in \mathscr{D} := \{d : d(\mathbf{x}, t) \in [0, 1]\}.$$

We denote the deformation gradient by $\mathbf{F} = \mathbf{I} + \nabla\mathbf{u}$, where $\nabla\cdot = \frac{\partial\cdot}{\partial\mathbf{x}}$ is the gradient operator defined with respect to the reference coordinates $\mathbf{x}$ and $\mathbf{I}$ is the unit tensor.

The variations $\tilde{\mathbf{u}}$ and $\tilde{d}$ will be used in the application of the minimality principle to derive the governing equations of the problem. These have to satisfy homogeneous boundary conditions, and as such belongs to the following sets

$$\tilde{\mathbf{u}}(\mathbf{x}, t) \in \widetilde{\mathscr{U}} := \{\tilde{\mathbf{u}}(\mathbf{x}, t) = \mathbf{0} \ \forall \mathbf{x} \in \partial\Omega_0^u\},$$

$$\tilde{d}(\mathbf{x}, t) \in \widetilde{\mathscr{D}} := \{\tilde{d} : \tilde{d}(\mathbf{x}, t) \geq 0 \ \text{for almost all} \ \mathbf{x} \in \Omega_0\},$$

the latter set being the convex cone of positive damage rate. As it will be apparent in the following sections, in the present formulation the damage variable can only increase (no–healing).

For the sake of conciseness the explicit dependence on the position $\mathbf{x}$ and time t will be omitted from all variables, except when needed.

2.2 Energy functional

The behaviour of the continuum is characterized at each material point $\mathbf{x}$ and at each time instant t by two state variables $\{\mathbf{u}, d\}$ in $\mathscr{U} \times \mathscr{D}$, and by a state function φ, which gives the energy density at each material point. As such, φ depends on the local strain $\mathbf{F}(\mathbf{x})$, on the value of the damage variable $d(\mathbf{x})$ and on the local value of damage gradient $\nabla d(\mathbf{x})$, with the following functional form

$$\varphi(\nabla\mathbf{u}, d, \nabla d) = \overbrace{\psi(\mathbf{I} + \nabla\mathbf{u}, d)}^{\text{Elastic energy}} + \overbrace{\underbrace{\frac{G_c}{c\,b}\eta(d)}_{\text{Dissipated energy}} + \underbrace{b\,\frac{G_c}{c}|\nabla d|^2}_{\text{Regularization}}}^{\text{Fracture energy}}, \qquad (2)$$

composed by three terms:

- $\psi(\mathbf{I} + \nabla \mathbf{u}, d)$ is the *elastic energy density* in the damage state d;

- $G_c \eta(d)/(c\,b)$ is the density of the *energy dissipated* during a homogeneous damage process with $\nabla d = 0$;

- $b\,G_c |\nabla d|^2/c$ is the *nonlocal* term which limits the possibility of damage localization without any energetic cost (see for instance [21]); such a term introduces an intrinsic length scale which controls the size of the damage localization zone.

The second and third terms in Eq. (2) constitute the *non-local fracture energy density*, in which the constitutive parameter G_c is the *critical elastic energy release rate*, b represents an internal length that regularizes the sharp crack and $c := 4 \int_0^1 \sqrt{\eta(d)}\, \mathrm{d}d$ is a scaling parameter [45].

We further assume that the elastic strain energy density ψ can be multiplicative decomposed as

$$\psi(\mathbf{I} + \nabla \mathbf{u}, d) = \omega(d)\, \psi_0(\mathbf{I} + \nabla \mathbf{u}), \tag{3}$$

in which $\psi_0(\mathbf{I} + \nabla \mathbf{u})$ is the elastic energy density of the neat material, and $\omega(d)$ is a monotonically decreasing energetic *degradation function* describing the degradation of the stored energy with evolving damage. The bulk strain energy density ψ_0 is a continuous isotropic function such that $\psi_0(\cdot)$ is frame indifferent. Such a requirement implies that, for any given deformation $\mathbf{F}$, one has $\psi_0(\mathbf{Q}^{\mathrm{T}} \mathbf{F} \mathbf{Q}) = \psi_0(\mathbf{F})$ (isotropic response) and $\psi_0(\mathbf{Q}^{\mathrm{T}} \mathbf{F}) = \psi_0(\mathbf{F})$ (frame indifference) for every rotation matrix $\mathbf{Q}$.

The energetic degradation function $\omega(d)$ plays an important role in determining the properties of the material, and, consistently with the experimental observation, we assume

$$\omega'(d) < 0 \quad \text{and} \quad \omega(0) = 1, \quad \omega(1) = 0, \quad \omega'(1) = 0,$$

where the latter constraint ensures that the energetic fracture converges to a finite value, if the damage converges to the fully broken state (see [22]).[1] Motivated by the analysis presented in [38], the following form for the degradation function ω is considered

$$\omega(d) := \frac{(1-d)^2}{(1-d)^2 + a_1\,d(1 + a_2\,d + a_2 a_3\,d^2)}, \tag{4}$$

---

[1] In the numerical examples carried out in Sec. 4 a small positive value of the degradation function is assumed when the material is fully broken. This is a standard technique to guarantee that the numerical problem remains well-posed for broken specimen.

where a_1, a_2 and a_3 are constitutive parameters, whose calibration allows the description of different fracture modes from brittle to pseudo-ductile. In Sec. 3 the constitutive coefficients of the fracture energy will be calibrated through uniaxial tests. As shown later, the chosen form of ω heavily affect the softening behaviour once crack is initiated.

The dissipated energy density plays a significant role in the evolution of the damage as well. We assume $\eta(d)$ to have the following quadratic expression

$$\eta(d) = 2\,d - d^2, \tag{5}$$

in a way that $\eta(0) = 0$ and $\eta(1) = 1$. With this assumption, the scaling parameter c becomes $c = 4 \int_0^1 \sqrt{2d - d^2}\, \mathrm{d}d = \pi$. We point out that different choices can be made for the function $\eta(d)$; the interested reader is referred to [38] for a full account of the different possibilities.

With the definition (2) of the state variable φ, we are in the position of defining the total energy stored in the material during the deformation process. For each admissible pair $(\mathbf{u}, d) \in \mathscr{U} \times \mathscr{D}$, the total energy of the continuum is

$$\mathcal{I}(\mathbf{u}, d) = \int_{\Omega_0} \varphi(\nabla\mathbf{u}, d, \nabla d) - \int_{\Omega_0} \mathbf{b}_0 \cdot \mathbf{u} - \int_{\partial\Omega_0^t} \mathbf{t}_0 \cdot \mathbf{u}, \tag{6}$$

$\mathbf{b}_0$ and $\mathbf{t}_0$ being the forces per unit of reference volume and area respectively, the latter applied on the part of the boundary $\partial\Omega_0^t$. These latter terms represent (minus) the work expended by the external forces.

Ogden–like strain energy   Considering the incompressibility of rubbery polymers, the elastic strain energy density that appears in (3) can be decomposed into isochoric and volumetric parts,

$$\psi_0(\mathbf{F}) = \psi_0^{\mathrm{iso}}(\overline{\mathbf{F}}) + U(J),$$

where $\overline{\mathbf{F}} = J^{-1/3}\mathbf{F}$ and $J = \det(\mathbf{F})$. In this contribution, however, we only consider *plane stress* cases meaning that the unknown pressure field associated to the incompressibility constraint $J = 1$ can always be determined via substitution in the out-of-plane deformation [46].

In the spirit of Ogden's phenomenological model, we formulate the strain energy density in terms of principal stretches λ_1, λ_2 and λ_3 of $\mathbf{F}$. In doing so, we set $J = 1$, and $\lambda_3 = (\lambda_1\lambda_2)^{-1}$ and we follow [2] on assuming the

8

following form[2] of ψ_0

$$\psi_0 = \phi(\lambda_1, \lambda_2) = \sum_{n=1}^{N} \frac{\mu_n}{\alpha_n}(\lambda_1^{\alpha_n} + \lambda_2^{\alpha_n} + (\lambda_1\lambda_2)^{-\alpha_n} - 3), \qquad (7)$$

where we have called ϕ the elastic energy density expressed in terms of the two independent principal stretches λ_1 and λ_2, from which we have omitted the dependence on $\mathbf{F}$. It is noted that the formulation (7) satisfies both frame invariance and isotropy.

In Eq. (7) N is a positive constant, usually $N = 3$ for most experiments on rubber, and μ_n and α_n are material constants such that $\mu_n\alpha_n > 0$ and $\sum_{n=1}^{N} \mu_n\alpha_n = 2\mu$, μ being the shear modulus of the material.

As a reference for the calculations in the next sections, we compute the Piola stress tensor, that is the dual quantity to $\nabla\tilde{\mathbf{u}}$ in the energetic formulation (11). With the definition of the Ogden's energy (7), and the hypothesis that $\lambda_3 = (\lambda_1\lambda_2)^{-1}$, we obtain

$$\mathbf{S} = \frac{\partial\psi}{\partial\mathbf{F}} = \omega\sum_{i=1}^{2} \phi_{,i}\, \mathbf{n}_i \otimes \mathbf{N}_i\,, \qquad \|\mathbf{n}_i\| = \|\mathbf{N}_i\| = 1, \qquad (8)$$

and

$$\phi_{,1} := \frac{\partial\phi}{\partial\lambda_1} = \sum_{n=1}^{N} \mu_n\big(\lambda_1^{\alpha_n-1} - (\lambda_1\lambda_2)^{-\alpha_n-1}\lambda_2\big)$$

$$\phi_{,2} := \frac{\partial\phi}{\partial\lambda_2} = \sum_{n=1}^{N} \mu_n\big(\lambda_2^{\alpha_n-1} - (\lambda_1\lambda_2)^{-\alpha_n-1}\lambda_1\big)$$

are the derivatives of the strain energy density $\phi(\lambda_1, \lambda_2)$ with respect to the principal stretches obtained by using the relationships reported in [3]. The directions $\{\mathbf{n}_1, \mathbf{n}_2, \mathbf{e}_3\}$ are the eigenvectors of the left stretch tensor $\mathbf{V}$ ($\mathbf{V}^2 = \mathbf{F}\mathbf{F}^{\mathrm{T}}$), and $\{\mathbf{N}_1, \mathbf{N}_2, \mathbf{e}_3\}$ are the ones of the right stretch tensor $\mathbf{U}$ ($\mathbf{U}^2 = \mathbf{F}^{\mathrm{T}}\mathbf{F}$), whereas $\mathbf{e}_3$ is assumed to be the direction of plane stress perpendicular either to $\{\mathbf{n}_1, \mathbf{n}_2\}$ and to $\{\mathbf{N}_1, \mathbf{N}_2\}$.

---

[2]Such an assumption is equivalent on assuming that the elastomer deforms in a perfectly incompressible way even after damage has occurred. This simplification could indeed be removed by coupling compressibility and damage growth, which however is not addressed in the present work.

2.3   Governing equations

The derivation of the governing equations of the problem, including the damage evolution, is carried out following the classical variational approach to fracture mechanics (see for instance [21] or [23]) which consists of:

1. the *damage irreversibility* condition $\dot{d}(\mathbf{x}, t) \geq 0$ and $d(\mathbf{x}, 0) = 0$,

2. a *stability criterion*, which is indeed a necessary condition for the unilateral minimality condition on the functional (6),

3. the *energy balance principle*, that states that the total energy at time t is equal to the work of the external forces up to time t.

A posteriori it is shown that, under the imposed constitutive assumptions, the *dissipation inequality*, that is the second principle of thermodynamics, is also satisfied.

Stability condition.   Starting from an undamaged state at $t = 0$, we say that the process evolves through stable equilibrium configurations if and only if at each time instant the system attains a local minimum of the total energy (6). This leads us on introducing the following *stability condition*:

For each $t > 0$, $\{\mathbf{u}, d\} \in \mathscr{U} \times \mathscr{D}$ is stable iff
$$\forall \{\tilde{\mathbf{u}}, \tilde{d}\} \in \widetilde{\mathscr{U}} \times \widetilde{\mathscr{D}}, \exists \bar{h} > 0 : \forall h \in [0, \bar{h}], \quad \mathcal{I}(\mathbf{u}, d) \leq \mathcal{I}(\mathbf{u} + h\tilde{\mathbf{u}}, d + h\tilde{d}), \tag{9}$$

with the initial condition $d(\mathbf{x}, 0) = 0$.

The variational inequality (9) is satisfied if the Gâteaux derivative of the functional $\mathcal{I}$ at $\{\mathbf{u}, d\}$ is positive for each set of test functions, in particular $\tilde{d}$ being in the convex cone defined by $\widetilde{\mathscr{D}}$. Formally we write

$$\mathcal{DI}(\mathbf{u}, d)[\tilde{\mathbf{u}}, \tilde{d}] \geq 0, \qquad \forall \{\tilde{\mathbf{u}}, \tilde{d}\} \in \widetilde{\mathscr{U}} \times \widetilde{\mathscr{D}}, \tag{10}$$

with

$$\mathcal{DI}(\mathbf{u}, d)[\tilde{\mathbf{u}}, \tilde{d}] = \int_{\Omega_0} \left(\mathbf{S} \cdot \nabla \tilde{\mathbf{u}} - \Sigma \, \tilde{d} + \mathbf{q} \cdot \nabla \tilde{d} \right) - \int_{\Omega_0} \mathbf{b}_0 \cdot \tilde{\mathbf{u}} + \int_{\Omega_0^t} \mathbf{t}_0 \cdot \tilde{\mathbf{u}}, \tag{11}$$

where the dual quantities $\mathbf{S}$, Σ and $\mathbf{q}$ are obtained from the energy density

(2) as

$$\mathbf{S} = \frac{\partial \psi}{\partial \mathbf{F}} = \omega \sum_{i=1}^{2} \phi_{,i}\, \mathbf{n}_i \otimes \mathbf{N}_i \qquad \text{(Piola stress tensor)} \qquad (12)$$

$$\Sigma = -\frac{\partial \varphi}{\partial d} = -\omega' \phi - \frac{G_c}{\pi b}\, \eta' \qquad \text{(Energy release rate density)} \quad (13)$$

$$\mathbf{q} = \frac{\partial \varphi}{\partial \nabla d} = \frac{2 G_c b}{\pi} \nabla d \qquad \text{(Damage flux vector)} \qquad (14)$$

the Piola stress $\mathbf{S}$ being given by the constitutive equation (8) in terms of the principal stretches λ_1, λ_2.

Upon substitution of (12)-(13)-(14) into (11) and integration by parts, the variational inequality (10) gives

$$\int_{\Omega_0} \big(\mathrm{Div}\, \mathbf{S} + \mathbf{b}_0 \big) \cdot \tilde{\mathbf{u}} + \int_{\partial \Omega_0^t} \big(\mathbf{t}_0 - \mathbf{S}\mathbf{n} \big) \cdot \tilde{\mathbf{u}} = 0, \qquad (15)$$

$$-\int_{\Omega_0} (\mathrm{Div}\, \mathbf{q} + \Sigma)\, \tilde{d} + \int_{\partial \Omega_0} (\mathbf{q} \cdot \mathbf{n})\, \tilde{d} \geq 0, \qquad (16)$$

where latter is evaluated as inequality since $\tilde{d}$ belongs to the convex cone $\widetilde{\mathscr{D}}$.

By the classical localization argument, we obtain from (15) the standard macroscopic balance equation with boundary conditions

$$\begin{aligned} \mathrm{Div}\, \mathbf{S} + \mathbf{b}_0 &= \mathbf{0}, \quad \text{on } \Omega_0, \\ \mathbf{S}\mathbf{n} &= \mathbf{t}, \qquad \text{on } \partial \Omega_0^t, \end{aligned} \qquad (17)$$

and from (16) the damage threshold condition

$$\begin{aligned} \mathrm{Div}\, \mathbf{q} + \Sigma &\leq 0, \quad \text{on } \Omega_0, \\ \mathbf{q} \cdot \mathbf{n} &\geq 0, \qquad \text{on } \partial \Omega_0, \end{aligned} \qquad (18)$$

with the corresponding flux condition on the boundary.

On using the definition of the energy release rate (13) and of the damage flux vector (14), we can rewrite the damage threshold condition $(18)_1$ as

$$f(\nabla \mathbf{u}, d, \Delta d) := \frac{G_c}{\pi} \Big(2\, b\, \Delta d - \frac{1}{b} \eta'(d) \Big) - \omega'(d) \psi_0(\mathbf{I} + \nabla \mathbf{u}) \leq 0, \qquad (19)$$

where we have defined the so-called *damage yield function* f. In the interior region where damage has yet to occur one has $\omega'(0)\psi_0(\mathbf{I} + \nabla \mathbf{u}) > -\frac{G_c}{\pi b}\eta'(0)$ and since $\omega'(d) < 0$ the elastic energy density ψ_0 is bounded.
We should remark once more that the damage threshold condition (19) is

indeed a necessary condition for the state $\{\mathbf{u}, d\}$ to be stable. Indeed if (19) is satisfied everywhere in the domain as a strict inequality, then the derivative (10) is strictly positive, and $\{\mathbf{u}, d\}$ is a stable state; on the other hand, if there are points in which the damage yield function is zero, then the stability of the state is given by the second derivative of the functional $\mathcal{I}$. This latter case will be discussed in Sec. 3 for the one-dimensional problem of a bar under traction.

Energy balance. On assuming that the evolution is smooth in time, the energy balance principle requires that the rate of the internal energy equals the working of external forces at each time instant, that is

$$\frac{d}{dt} \int_{\Omega_0} \varphi(\nabla \mathbf{u}, d, \nabla d) = \int_{\Omega_0} \mathbf{b}_0 \cdot \dot{\mathbf{u}} + \int_{\Omega_0^t} \mathbf{t}_0 \cdot \dot{\mathbf{u}}, \qquad (20)$$

which, upon using the macroscopic balance (17), gives

$$\int_{\Omega_0} -\left(\mathrm{Div}\,\mathbf{q} + \Sigma\right) \dot{d} + \int_{\partial \Omega_0} \left(\mathbf{q} \cdot \mathbf{n}\right) \dot{d} = 0.$$

Since each integrand is non negative by the balance equation (18), and the damage irreversibility condition requires that $\dot{d} \geq 0$, the above energy balance equation is satisfied if its integrands vanish. These requests give the Kuhn-Tucker conditions for the threshold function (19):

$$\begin{cases} f(\nabla \mathbf{u}, d, \Delta d) = 0, & \text{if } \dot{d} > 0, \\ f(\nabla \mathbf{u}, d, \Delta d) < 0, & \text{if } \dot{d} = 0, \end{cases} \qquad (21)$$

supplemented by Neumann-type boundary condition $\nabla d \cdot \mathbf{n} = 0$ on $\partial \Omega_0$.

Remark 1 (Evolution problem). The evolution problem arising from stability condition and energy balance is usually solved numerically in an incremental form. The problem is discretized in time, and at each time step the rates $\{\dot{\mathbf{u}}, \dot{d}\}$ are computed through a staggered minimization scheme obtained by alternating the minimization between $\dot{\mathbf{u}}$ and $\dot{d}$, keeping the other variable constant. This numerical procedure is indeed a standard approach to solve variational problems like the present one (see for instance [47]).

Remark 2 (Energy dissipation). In the framework introduced above, the free energy is the sum of the elastic energy and of the non–local fracture

energy, that is

$$\mathcal{F} = \int_{\Omega_0} \left(\omega\,\phi + \frac{1}{\pi} G_c b |\nabla d|^2 \right).$$

The second principle of thermodynamics requires that, for each admissible state $\{\mathbf{u}, d\}$, the internal working be equal to or larger than the rate of the free energy, i.e.,

$$\delta = \int_{\Omega_0} \mathbf{S} \cdot \nabla\dot{\mathbf{u}} - \frac{\mathrm{d}}{\mathrm{d}t}\mathcal{F} \geq 0. \tag{22}$$

On using the definition of the Piola stress tensor (8), the Neumann boundary condition $\nabla d \cdot \mathbf{n} = 0$, and on integrating by parts, Eq. (22) simplifies to

$$\delta = \int_{\Omega_0} \left(\frac{2}{\pi} G_c b \Delta d - \omega'\phi \right) \dot{d} \geq 0,$$

which is zero when $\dot{d} = 0$, whereas when damage evolves one obtains

$$\delta = \int_{\Omega_0} \frac{G_c}{\pi\,b} \eta' \dot{d} > 0,$$

that is positive since $\eta' = 2(1 - d) > 0$ from the definition in Eq. (5).

Remark 3 (Internal length). The internal length b in Eq. (2) can be related to the damage bandwidth ℓ_f at complete fracture, that is the support of the damage function when $\max\{d\} = 1$, by solving the equilibrium problem of a fractured bar with a passing-through transversal crack. In this case, strains vanish because the bar is broken into two parts, and the strain energy density ϕ nullifies. Thus the balance equation $(21)_1$ reduces to $2\,b\,\Delta d - \frac{1}{b}\eta'(d) = 0$. On integrating it over a line orthogonal to the crack surface (see [21] or [38] for details on the calculation), it gives

$$b = \frac{\ell_f}{2 \int_0^1 \frac{1}{\sqrt{\eta(d)}}\mathrm{d}d},$$

that, by assuming the quadratic expression of $\eta(d)$ in (5), reduces to

$$b = \frac{\ell_f}{\pi}.$$

13

2.4 Recap of all modelling equations

By following the classical approach to variational fracture mechanics enunciated in the three principles 1., 2. and 3. of Sec. 2.3 we have arrived at the following equations governing the macroscopic balance

$$
\boxed{
\begin{aligned}
\text{Macroscopic balance:} \quad & \text{Div}\,\mathbf{S} + \mathbf{b}_0 = \mathbf{0} && \text{on } \Omega_0 \\
& \mathbf{S}\mathbf{n} = \mathbf{t}_0 && \text{on } \partial\Omega_0
\end{aligned}
}
\tag{23}
$$

together with Kuhn-Tucker conditions for the damage evolution problem

$$
\boxed{
\begin{aligned}
\text{Damage irreversibility:} \quad & \dot{d}(\mathbf{x},t) \geq 0 \\
\text{Damage threshold:} \quad & f(\nabla\mathbf{u}, d, \Delta d) \leq 0 \\
\text{Energy balance:} \quad & f(\nabla\mathbf{u}, d, \Delta d)\dot{d} = 0
\end{aligned}
}
\tag{24}
$$

with initial condition $d(\mathbf{x},0) = 0$. The Piola stress tensor $\mathbf{S}$ and the damage threshold function f are

$$
\mathbf{S} = \omega \sum_{i=1}^{2} \phi_{,i}\, \mathbf{n}_i \otimes \mathbf{N}_i \,,
$$

$$
f = G_c\Big(\frac{2}{\pi^2}\,\ell_f\,\Delta d - \frac{1}{\ell_f}\eta'\Big) - \omega'\phi \,,
$$

with $\mathbf{n}_i$ and $\mathbf{N}_i$ eigenvectors of the left and right Cauchy–Green strain tensors, and

$$
\phi = \sum_{n=1}^{N} \frac{\mu_n}{\alpha_n}(\lambda_1^{\alpha_n} + \lambda_2^{\alpha_n} + (\lambda_1\lambda_2)^{-\alpha_n} - 3) \,,
$$

$$
\omega = \frac{(1-d)^2}{(1-d)^2 + a_1\,d(1 + a_2\,d + a_2 a_3\,d^2)} \,,
\tag{25}
$$

$$
\eta = 2\,d - d^2 \,.
$$

The constitutive parameters included into the formulation are the elastic moduli μ_n and exponents α_n of the strain energy density ϕ, the fracture energy release rate G_c, the internal length ℓ_f, and the polynomial coefficients a_1, a_2 and a_3 of the degradation function ω. In the next Sect. 3.5, strategies to calibrate the constitutive parameters are discussed.

3   1D tension test

In order to fully exploit the capabilities of the proposed model, we now study the problem of a bar under tension. Such a simplified example will allows us to solve the governing equations in semi-analytical form, and assess thoroughly the role of the different constitutive coefficients that appears in the model.

3.1   Problem definition

We consider a bar of length ℓ and cross-section area $\mathcal{A}_0$. The reference configuration is described through a triad of orthonormal vector $\{\mathbf{e}_1, \mathbf{e}_2, \mathbf{e}_3\}$, with $\mathbf{e}_1$ being the main axis of the bar and $\mathbf{e}_3$ the thickness direction, i.e.,

$$\Omega_0 = \{\mathbf{x} : \mathbf{x} = x_1\,\mathbf{e}_1 + x_2\,\mathbf{e}_2 + x_3\,\mathbf{e}_3,\ x_1 \in (0, \ell), (x_2, x_3) \in \mathcal{A}_0\}.$$

To solve the equilibrium problem, we make the following *ansätze* on the deformation gradient

$$\mathbf{F}(x_1) = \lambda(x_1)\,\mathbf{e}_1 \otimes \mathbf{e}_1 + \frac{1}{\sqrt{\lambda(x_1)}}\,\big(\mathbf{e}_2 \otimes \mathbf{e}_2 + \mathbf{e}_3 \otimes \mathbf{e}_3\big), \qquad (26)$$

such that the principal stretches are $\lambda_1 = \lambda(x_1)$, $\lambda_2 = \lambda_3 = (\lambda(x_1))^{-1/2}$, $J = 1$, and all fields depend only on the longitudinal coordinate x_1, which, from now on, we call x without the risk of confusion.

The displacement of the bar axis is $u(x)$, and the longitudinal stretch $\lambda(x)$ can be computed from the latter *via*

$$\lambda(x) = 1 + u'(x), \qquad (27)$$

with the boundary conditions

$$u(0) = 0, \quad u(\ell) = \varepsilon\ell,$$

with $\varepsilon \geq 0$ a control parameter, that represents the dimensionless displacement applied at the right end side of the bar. In (27) we have indicated with a prime $\prime$ the derivative with respect to the variable x.

We assume the damage field to be constant within the bar cross-section, so that it depends only on the abscissa x, i.e., $d = d(x)$ and satisfies homogeneous boundary conditions at both ends, i.e.,

$$d(0) = d(\ell) = 0,$$

meaning that no crack can appear at the extremities. Indeed, cracks near the clamping are avoided in the experiments by using dog-bone shaped specimen.

In this 1D-setting, the energy density of the bar takes the following form

$$\varphi(\lambda, d, d') = \omega(d)\hat{\phi}(\lambda) + G_c\Big(\frac{1}{\ell_f}\eta(d) + \frac{\ell_f}{\pi^2}\, d'^2\Big),$$

where we have indicated by $\hat{\phi}(\lambda) = \phi(\lambda, \lambda^{-1/2})$ the reduced strain energy density of the bulk solid defined in Eq. (7) as a function of the only variable λ. For the sake or readability the hat will be dropped in the following.

The stress field corresponding to the deformation gradient (26) can be computed from (8) on substituting $\lambda_1 = \lambda$ and $\lambda_2 = \lambda^{-1/2}$ and on noting that the right- and left- eigenvectors coincide, i.e., $\mathbf{n}_1 = \mathbf{N}_1 = \mathbf{e}_1$, $\mathbf{n}_2 = \mathbf{N}_2 = \mathbf{e}_2$. The only non zero component of the Piola stress is the one directed along the bar main axis, i.e., $S = \mathbf{S}\,\mathbf{e}_1 \cdot \mathbf{e}_1$, with

$$S = \omega\phi', \tag{28}$$

that, by applying the definition of the Ogden's strain energy density, gives

$$S = \omega \sum_{n=1}^{N} \frac{\mu_n}{\lambda}\big(\lambda^{\alpha_n} - \lambda^{-\frac{\alpha_n}{2}}\big).$$

The macroscopic balance equation (17) can be rewritten as

$$S'(x) = 0, \tag{29}$$

meaning that the stress is constant along the bar. The reduced damage threshold condition $(24)_2$ with the deformation (26) yields the following form of the one-dimensional threshold function

$$f(\lambda, d, d'') = G_c\Big(\frac{2\ell_f}{\pi^2}\, d'' - \frac{1}{\ell_f}\eta'(d)\Big) - \omega'(d)\phi(\lambda) \leq 0. \tag{30}$$

3.2 Incremental Evolution

Following the analysis in [48], we now solve the incremental evolution problem for both displacement and damage variables starting from a known solution $\{u, d\}$ achieved at a certain time instant t. In doing so, we assume a uniform discretization of the time axis, we call τ the time step, and we expand both displacement and damage fields at the first order in τ:

$$u(x, t+\tau) = u(x, t) + \tau\,\dot{u}(x, t), \quad d(x, t+\tau) = d(x, t) + \tau\,\dot{d}(x, t), \tag{31}$$

16

such that

$$\dot{u}(0,t) = 0, \quad \dot{u}(\ell,t) = \dot{\varepsilon}\ell, \quad \dot{d}(0,t) = 0, \quad \dot{d}(\ell,t) = 0. \tag{32}$$

with $\dot{\varepsilon}$ the rate of the applied displacement at the right end of the bar.

At each time instant the solution of the incremental problem requires the evaluation of the unknown rates $\{\dot{u}, \dot{d}\}$ obtained by imposing the stability condition (10) and the energy balance condition (21) for the solution $\{u + \tau\dot{u}, d + \tau\dot{d}\}$.

The total energy functional (6), with null volume forces, is expanded at the second order as

$$\mathcal{I}(u+\tau\dot{u}, d+\tau\dot{d}) \simeq \mathcal{I}(u,d) + \tau \, \dot{\mathcal{I}}(u,d,\dot{u},\dot{d}) + \frac{1}{2}\tau^2 \, \ddot{\mathcal{I}}(u,d,\dot{u},\dot{d}) = \mathcal{I}(u,d) + \tau \, \mathcal{J}(\dot{u},\dot{d}), \tag{33}$$

in which we have defined the following functional of the displacement and damage rates

$$\mathcal{J}(\dot{u},\dot{d}) = \mathcal{A}_0 \int_0^\ell \left[\omega\phi'\dot{u}' + (\omega'\phi + \frac{G_c}{\ell_f}\eta')\dot{d} + \frac{2}{\pi^2}G_c\ell_f d'\dot{d}' \right] dx$$

$$+ \frac{1}{2}\tau\mathcal{A}_0 \int_0^\ell \left[\omega\phi''\dot{u}'^2 + (\omega''\phi + \frac{G_c}{\ell_f}\eta'')\dot{d}^2 + 2\omega'\phi'\dot{u}'\dot{d} + \frac{2}{\pi^2}G_c\ell_f\dot{d}'^2 \right] dx. \tag{34}$$

Stability and energy balance, expressed by relations (10) and (20) in the three-dimensional formulation of Sec. 2, are rewritten in the following form

$$\mathcal{D}\mathcal{J}(\dot{u},\dot{d})[\tilde{u},\tilde{\dot{d}}] \geq 0, \text{ for any } \{\tilde{u}, \tilde{\dot{d}}\} \text{ such that } \tilde{u} = \tilde{\dot{d}} = 0 \text{ at } x = 0, l, \text{ and } \tilde{\dot{d}} \geq 0,$$

$$\frac{d}{d\tau}\mathcal{I}(u + \tau\dot{u}, d + \tau\dot{d}) = \frac{d}{d\tau}\left(\tau \, \mathcal{J}(\dot{u},\dot{d})\right) = 0.$$

By performing calculations analogous to those followed in Sect. 2.3 to deduce the governing equations (17) and (18) from the stability condition (10), and the evolution relations (21) from the energy balance (20), we obtain the following macroscopic evolution equation

$$S' + \tau\dot{S}' = \frac{d}{dx}(\omega\phi') + \tau\frac{d}{dx}(\omega\phi''\dot{u}' + \omega'\phi'\dot{d}) = 0, \tag{35}$$

together with the set of Kuhn-Tucker conditions that govern the evolution of the damage field

$$\dot{d} \geq 0, \quad f + \tau\dot{f} \leq 0, \quad (f + \tau\dot{f})\,\dot{d} = 0, \tag{36}$$

17

with $\dot{f}$ computed from (30) as

$$\dot{f} = -\omega'\phi'\dot{\lambda} - \left(\frac{G_c}{\ell_f}\eta'' + \omega''\phi\right)\dot{d} + \frac{2}{\pi^2}G_c\ell_f\dot{d}''.$$

These conditions state that, at each point, the damage can increase only if the yield function $f + \tau\dot{f}$ is equal to zero.

3.3 Damage onset

At the beginning of the loading process the damage is zero, and the bar is stretched elastically. The balance equation (29) shows that the stress and the corresponding deformation are homogeneous along the bar. In this initial phase the damage yield condition (30) is not satisfied, i.e., $f < 0$.

The elastic stage terminates when damage appears, meaning that $f = 0$ somewhere along the bar. The stretch λ_o corresponding to the damage onset is evaluated from (30) as

$$\phi(\lambda_o) = -\frac{G_c}{\ell_f}\frac{\eta'(0)}{\omega'(0)}. \tag{37}$$

At this time instant, say t_o, one can solve the incremental evolution problem of Sec. 3.2 by assuming the following form of the series expansion (31)

$$u(x, t_o + \tau) = \varepsilon(t_o)x + \tau\,\dot{u}_o(x), \qquad d(x, t_o + \tau) = \tau\,\dot{d}_o(x),$$

since the stretch at the onset is homogeneous, $\lambda_o = 1 + \varepsilon(t_o)$, and the damage is null, $d(x, t_o) = 0$; in addition, $\dot{u}_o$ and $\dot{d}_o$ satisfy the boundary conditions (32). At the step $t_o + \tau$, the stretch becomes $\lambda(x, t_o + \tau) = 1 + \varepsilon_o + \tau\,\dot{\lambda}_o(x)$, such that $\dot{\lambda}_o(x) = \dot{u}'_o(x)$, which is a function of x due to the varying damage profile. A subscript "o" is used to indicate, here and henceforth, that the corresponding variable is evaluated at time t_o.

The incremental stress in the bar is approximated at the first order in τ from the definition of the one-dimensional Piola stress (28)

$$S = \omega(\tau\dot{d}_o)\,\phi'(\lambda_o + \tau\dot{\lambda}_o) \simeq S_o + \tau\,\dot{S}_o,$$

with

$$S_o = \phi'_o, \quad \text{and} \quad \dot{S}_o = \omega_o\,\phi'_o\,\dot{d}_o + \phi''_o\,\dot{\lambda}_o. \tag{38}$$

Since the zero order stress S_o is constant along the bar, the macroscopic balance (35) yields $(\dot{S}_o)' = 0$, meaning that also $\dot{S}_o$ is homogeneous. The damage threshold condition $f = 0$ is verified both at $t = t_o$ and $t = t_o + \tau$,

thus the incremental threshold (36) is zero at both zero-th and first orders; the latter gives

$$\frac{2}{\pi^2} G_c \, \ell_f \, \dot{d}_{\mathrm{o}}{}''(x) - \left(\omega_{\mathrm{o}}'' \phi_{\mathrm{o}} + \frac{G_c}{\ell_f} \eta_{\mathrm{o}}''\right) \dot{d}_{\mathrm{o}}(x) = \phi_{\mathrm{o}}' \, \dot{\lambda}_{\mathrm{o}}(x) \qquad (39)$$

which is, indeed, a second order differential equation for the damage rates $\{\dot{\lambda}_{\mathrm{o}}, \dot{d}_{\mathrm{o}}\}$. The rhs of (39) can be transformed by using the definition of $\dot{S}_{\mathrm{o}}$ in (38); after some manipulations we arrive at differential equation of the only variable $\dot{d}_{\mathrm{o}}$:

$$\frac{2}{\pi^2} G_c \, \ell_f \, \dot{d}_{\mathrm{o}}{}''(x) - j \dot{d}_{\mathrm{o}}(x) = \frac{\omega_{\mathrm{o}}' \phi_{\mathrm{o}}'}{\phi_{\mathrm{o}}''} \dot{S}_{\mathrm{o}}, \qquad \text{with} \quad j = \omega_{\mathrm{o}}'' \phi_{\mathrm{o}} - \frac{\omega_{\mathrm{o}}'^2 \phi_{\mathrm{o}}'^2}{\phi_{\mathrm{o}}''} + \frac{G_c}{\ell_f} \eta_{\mathrm{o}}''. \tag{40}$$

where the rhs is now independent of x. Equation (40) is a second order differential equation in the variable x of the unknown rate $\dot{d}_{\mathrm{o}}$ to be solved with the boundary conditions $\dot{d}_{\mathrm{o}}(0) = 0$ and $\dot{d}_{\mathrm{o}}(\ell) = 0$.

An equation similar to (40) was already studied in [48] for a small strain model (see equation (31) in [48]). The solution strategy exploited there can be equally applied to the large strain analysis carried out in this paper. In particular, the following steps allows us to calculate the unknown rates $\{\dot{u}_{\mathrm{o}}, \dot{d}_{\mathrm{o}}\}$: (i) first $\dot{d}_{\mathrm{o}}$ is determined in terms of $\dot{S}_{\mathrm{o}}$ by solving (40); thereafter (ii) $\dot{S}_{\mathrm{o}}$ is determined by evaluating the mean value, i.e., $< \cdot > = \frac{1}{\ell} \int_0^\ell \cdot \mathrm{d}x$, of both the sides of Eq. $(38)_2$, that gives

$$\dot{S}_{\mathrm{o}} = \omega_{\mathrm{o}}' \, \phi_{\mathrm{o}}' < \dot{d}_{\mathrm{o}} > + \phi_{\mathrm{o}}'' \, \dot{\varepsilon}_o, \tag{41}$$

where we made use of the fact that $\dot{S}_{\mathrm{o}}$ is constant along the bar and $< \dot{\lambda}_{\mathrm{o}} > = \dot{\beta}$ by the boundary condition (32); finally, (iii) u is determined by integration of $(38)_2$ expressed in terms of $\dot{\lambda}_{\mathrm{o}} = \dot{u}_{\mathrm{o}}'$.

To distinguish the different evolution regimes, we introduce the internal lengths ℓ_i and ℓ_s defined by

$$\ell_i = 2\sqrt{\frac{2G_c \, \ell_f}{|j|}}, \quad \ell_s = \frac{\omega_{\mathrm{o}}'^2 \phi_{\mathrm{o}}'^2}{\phi_{\mathrm{o}}'' |j|} \, \ell_i,$$

which allow us to rewrite Eq. (40) in the following form

$$\dot{d}_{\mathrm{o}}{}''(x) - \operatorname{sign}(j) \left(\frac{2\pi}{\ell_i}\right)^2 \dot{d}_{\mathrm{o}}(x) = \left(\frac{2\pi}{\ell_i}\right)^2 \sqrt{\frac{\ell_s}{\ell_i}} \frac{\dot{S}_{\mathrm{o}}}{\sqrt{\phi_{\mathrm{o}}'' |j|}} \; .$$

Fracture initiation is *full-size*, when the support of $\dot{d}_{\mathrm{o}}$ is the entire bar, or *localized* in a subregion, if $\ell_i < \ell$. The evolution of the damage is *stress-hardening* when $\dot{S}_{\mathrm{o}} > 0$ or *stress-softening* when $\dot{S}_{\mathrm{o}} < 0$. In particular, the evolution problem was solved in the following sub-cases:

a. For $j \geq 0$, the solution obtained by applying the procedure (i), (ii) and (iii) is

$$\dot{d}_{\mathrm{o}}(x) = -\frac{\omega'_{\mathrm{o}}\phi'_{\mathrm{o}}}{j(1+ <g> \ell_s/\ell_i)}\dot{\varepsilon}_{\mathrm{o}} \, g(x), \quad \text{and} \quad \dot{S}_{\mathrm{o}} = \frac{\phi''}{1+ <g> \ell_s/\ell_i}\dot{\varepsilon}_{\mathrm{o}},$$

with

$$g(x) = 1 - \frac{\cosh\left(\pi(\ell - 2x)/\ell_i\right)}{\cosh(\pi\ell/\ell_i)}, \quad \text{and} \quad <g> = 1 - \frac{\ell_i}{\pi\ell} \tanh\left(\frac{\pi\ell}{\ell_i}\right).$$

Damage evolution is *full-size* in a regime of *stress-hardening*.

b. For $j < 0$ and $\ell_i \geq \ell$, the solution is

$$\dot{d}_{\mathrm{o}}(x) = -\frac{\omega'\phi'}{j(1- <g> \ell_s/\ell_i)}\dot{\varepsilon}_{\mathrm{o}} g(x), \quad \text{and} \quad \dot{S}_{\mathrm{o}} = \frac{\omega\phi''_{\mathrm{o}}}{1- <g> \ell_s/\ell_i}\dot{\varepsilon}_{\mathrm{o}} \tag{42}$$

with

$$g(x) = 1 - \frac{\cos\left(\pi(\ell - 2x)/\ell_i\right)}{\cos(\pi\ell/\ell_i)}, \quad \text{and} \quad <g> = 1 - \frac{\ell_i}{\pi\ell} \tan\left(\frac{\pi\ell}{\ell_i}\right).$$

Solution $\dot{d}_{\mathrm{o}}$ is *full-size* and two evolution regimes are obtained:

b.1. if $\ell_i > 2\ell$, the regime is *stress-hardening*, since $<g> < 0$;

b.2. if $\ell < \ell_i \leq 2\ell$, the regime is *stress-softening*, being $<g> > 0$. In this case, the condition

$$<g> \geq \ell_i/\ell_s \tag{43}$$

must be satisfied to have $\dot{d}_{\mathrm{o}} \geq 0$ everywhere.

c. For $j < 0$ and $\ell_i < \ell$, the solution has the expression (42), with

$$g(x) = \begin{cases} 1 - \cos(2\pi x/\ell_i), & \text{if } 0 < x < \ell_i, \\ 0, & \text{if } x \geq \ell_i, \end{cases} \quad \text{and} \quad <g> = \ell_i/\ell.$$

and so is localized in a portion of length ℓ_i (*localized solution*), and the evolution regime is *stress-softening*. Even in this case, the inequality

$$\ell \leq \ell_s \tag{44}$$

has to be fulfilled to have $\dot{d}_{\mathrm{o}} \geq 0$.

20

It can be proved that inequalities (43) and (44) are necessary conditions for stability of the evolution problem (see [48]); indeed they guarantee non-negativeness of the second variation of the functional (34). If stability conditions are not satisfied, the bar fails catastrophically at the time instant t_o, experiencing brittle fracture.

In case c., the bar must be longer than ℓ_i to have damage localization in a sub-region of length ℓ_i, and smaller than ℓ_s to avoid brittle failure. These requirements express the size sensitivity of the model: as the size of the bar increases, the response moves from ductile to brittle. If we suppose damage localization at t_o, the slope k_o of the curve $S = S(\varepsilon)$ is obtained from the solution in Eq. $(42)_2$, with $<g>= \ell_i/\ell$,

$$k_o = \frac{dS}{d\varepsilon}\bigg|_{t_o} = \frac{\dot{S}_o}{\dot{\varepsilon}_o} = \frac{\omega_o \phi_o''}{1 - \ell_s/\ell}, \tag{45}$$

that has a negative value and decreases as ℓ increases; in particular $k_o \to -\infty$ for $\ell \to \ell_s$.

On integrating (41) over $(0, \ell)$ and rearranging the terms, we obtain the displacement rate at the end-section

$$\dot{u}_o(\ell) = \ell\dot{\varepsilon}_o = \dot{v}_o + \dot{w}_o \quad \text{with } \dot{v}_o = \ell\frac{\dot{S}_o}{\phi_o''}, \text{ and } \dot{w}_o = -\ell\frac{\omega_o' \phi_o'}{\phi_o''}<\dot{d}_o>,$$

which is the sum of two contributions: $\dot{v}_o$ is the displacement rate due to elastic stretching, and $\dot{w}_o$ is the displacement rate induced by the fracture opening. In case of localized $\dot{d}_o$ (case c., with $\ell_i \leq \ell \leq \ell_s$), the fracture opening rate is

$$\dot{w}_o = \frac{\ell_s}{1 - \ell_s/\ell}\dot{\varepsilon}_o. \tag{46}$$

Let $w = w(t)$ be the displacement accounting for fracture opening in a fracture evolution process. Using $(42)_2$ and (46), we can evaluate the derivative of S with respect to w at fracture initiation as

$$\hat{k}_o = \frac{dS}{dw}\bigg|_{t_o} = \frac{\dot{S}_o}{\dot{w}_o} = -\frac{\phi_o''}{\ell_s}. \tag{47}$$

The coefficient $\hat{k}_o$ represents the initial slope of the so-called *cohesive curve* $S = S(w)$, which describes the specific failure mode of the material. Since the cohesive law $S = S(w)$ is an intrinsic property of the material, $\hat{k}_o$ does not depend on the length ℓ, differently from (45).

21

3.4 Cohesive fracture

In this section we define a strategy to estimate the cohesive curve $S = S(w)$, that characterizes the fracture opening process. The function $S(w)$ is usually assigned a-priori in standard formulations of cohesive fracture mechanics [49, 50]), whereas in the proposed variational approach is obtained from the peculiar form of the fracture energy.

We suppose that, at a certain time instant of the evolution process, damage is localized in a sub-region $(0, 2x^*)$, with $x^* < \ell/2$ the half-bandwidth length, and that it has attained the maximum value d^* at $x = x^*$. The proposed procedure allows us to determine the length x^*, the stress S, the functions d and λ, the fracture opening w, as well as the corresponding strain ε in terms of d^* by integrating the balance equations (29) and (30).

We suppose that, at each material point, the stretch λ is the superposition of an elastic λ_e and fracture λ_f stretches

$$\lambda = \lambda_f \, \lambda_e,$$

where λ_e would be the homogeneous stretch obtained from S if d were zero; as such, it can be evaluated from the constitutive equation of the undamaged material by

$$\phi'(\lambda_e) = S.$$

The fracture opening w, that is the displacement at $x = \ell$ produced by the damage occurrence is

$$w = \int_0^{\lambda_e \ell} \big(\lambda_f(x_e) - 1\big) \mathrm{d}x_e = \int_0^\ell (\lambda - \lambda_e) \, \mathrm{d}x = (1 + \varepsilon)\ell - \lambda_e \ell. \qquad (48)$$

Within the damage region $(0, 2x^*)$, the damage threshold condition (30) is evaluated as an equality and

$$\omega'\phi + G_c \left(\frac{1}{\ell_f}\eta' - \frac{2\ell_f}{\pi^2}d'' \right) = 0,$$

On multiplying all terms by d' and on integrating over $(0, x)$, with $x \le x^*$, previous equation gives

$$G_c \left(\frac{1}{\ell_f}\eta - \frac{2\ell_f}{\pi^2}d'^2 \right) + \int_0^x \frac{\mathrm{d}\omega}{\mathrm{d}\hat{x}}\phi \, \mathrm{d}\hat{x} = 0. \qquad (49)$$

where the latter term is rewritten by integration by parts as

$$\int_0^x \frac{\mathrm{d}\omega}{\mathrm{d}\hat{x}}\phi \, \mathrm{d}\hat{x} = \omega\phi - \phi(\lambda_e) - \int_0^x \omega\phi' \frac{\mathrm{d}\lambda}{\mathrm{d}\hat{x}} \, \mathrm{d}\hat{x} = \omega\phi - \phi(\lambda_e) - (\lambda - \lambda_e)S,$$

since $S = \omega\phi'$ is constant along the bar. Equation (49) becomes

$$G_c \left(\frac{1}{\ell_f} \eta - \frac{2\ell_f}{\pi^2} d'^2 \right) + \omega\phi - \phi(\lambda_e) - (\lambda - \lambda_e)S = 0. \tag{50}$$

At $x = x^*$, where the maximum damage is attained, $d'(x^*) = 0$ and previous equation further simplifies into

$$\frac{G_c}{\ell_f} \eta(d^*) + \omega(d^*)\phi(\lambda^*) - \phi(\lambda_e) - (\lambda^* - \lambda_e)S^* = 0, \tag{51}$$

where quantities evaluated at $x = x^*$ are labelled by an asterisk. In (51), the stretches λ^* and λ_e are worked out by inversion of the constitutive equations

$$\omega(d^*)\phi'(\lambda^*) - S^* = 0, \quad \phi'(\lambda_e) - S^* = 0. \tag{52}$$

For any assigned value of $d^* \in [0, 1]$, the triplet $\{\lambda^*, \lambda_e, S^*\}$ solves the set of equations (51) and (52). Once S^* is determined, the profiles of d and λ at points $x \in [0, x^*]$ can be evaluated from (50), here rewritten in the following form

$$d' = \frac{1}{\ell_f} h(d, d^*), \quad \text{with} \quad h(d, d^*) := \pi\sqrt{\frac{\ell_f}{G_c} [\omega(d)\phi(\lambda) - \phi(\lambda_e) - f^*(\lambda - \lambda_e)] + \eta}, \tag{53}$$

where λ is the solution of the equation

$$\omega(d)\phi'(\lambda) - S^* = 0. \tag{54}$$

Upon inversion of Eq. (53), one obtains the expression of x in terms of the damage profile and of the maximum damage d^*,

$$x(d, d^*) = \int_0^d \frac{\ell_f}{h(\hat{d}, d^*)} \, \mathrm{d}\hat{d}, \tag{55}$$

and the stretch λ at x is the solution of (54). The half-bandwidth length is obtained from the above relation by assigning $d = d^*$

$$x^* = \int_0^{d^*} \frac{\ell_f}{h(\hat{d}, d^*)} \, \mathrm{d}\hat{d},$$

and the fracture opening w is determined from (48), once λ, λ_e and x^* are known. Upon inversion of the equation, also the assigned stretch can be computed

$$\varepsilon = \lambda_e + \frac{w}{\ell} - 1.$$

To conclude, the above procedure can be implemented numerically through the following steps:

i. Assign the value d^* of the maximum damage.

ii. Solve equations (51) and (52) to determine S^*, λ^* and λ_e.

iii. Discretize the damage range $[0, d^*]$, and, for any d_i of the discretized set, determine the position x_i from (55). The discrete profile of $d = d(x)$ is given by the pairs (x_i, d_i).

iv. Determine λ_i at point x_i from (54). The discrete profile of $\lambda = \lambda(x)$ is drawn by points (x_i, λ_i). At points $x > 2x^*$ the stretch is equal to λ_e.

v. Determine w from (48).

With previous algorithm, the cohesive curve $S = S(w)$ is evaluated at discrete points, by iterating the previous scheme for different values of $d^* \in [0, 1]$. The damage evolution determined through this procedure is based on the balance equations (29) and (30). It is pointed out that the numerical simulations of Sec. 4 are indeed obtained by solving the full evolution problem of Sec. 3.2 by finite elements. Although the approaches are different, the estimate of the cohesive curve obtained through steps $(i) - (v)$ gave accurate enough results to catch the qualitative behaviour of the model. As such, the proposed numerical scheme represents an useful tool to explore the variety of damage mechanisms that can be captured. In the next section, these results are used to assess the effects of the different constitutive parameters on the damage evolution modes. Criteria for parameters calibration will be also discussed.

3.5 Physical interpretation of the cohesive parameters

The constitutive coefficients a_1, a_2 and a_3 that appear in the energy degradation function ω, as defined in (4), are put in relation to specific properties of cohesive fracture evolution, to give them a clear physical meanings and to allow their robust evaluation from the experimental data. In the following calculations, the elastic coefficients μ_n and α_n, the fracture energy release rate G_c, and the internal length ℓ_f are supposed to be known.

The coefficients a_1, a_2 in (4) can be tailored from the model response at the damage onset. At this time instant $\lambda_f = 1$, $\lambda_e = \lambda_o$ and the stress S_o is known. Since $d_o = 0$, the functions ω and η at t_o are

$$\eta(0) = \omega(0) = 0, \quad \eta'(0) = 2, \quad \omega'(0) = -a_1, \quad \eta''(0) = -2, \quad \omega''(0) = 2a_1(a_1 - a_2 - 2).$$

1. The coefficient a_1 is determined by the limit elastic stretch λ_o through relation (37), which, once inverted, gives

$$a_1 = 2\frac{G_c}{\phi_o\,\ell_f}. \tag{56}$$

2. The coefficient a_2, that appears in $\omega''(0)$, is made dependent on the slope $\hat{k}_o$ of the cohesive curve (47) at the damage onset, i.e.,

$$\hat{k}_o = -\frac{\phi_o''^2}{2a_1^2 S_o^2}\sqrt{\frac{|j|^3}{2\,G_c\,\ell_f}}, \quad \text{with} \quad j = 2a_1(a_1 - a_2 - 2)\phi_o - \frac{a_1^2 S_o^2}{\phi_o''} - \frac{2G_c}{\ell_f}, \tag{57}$$

where j is negative, as the formula is evaluated for the localized damage case (case c. in Sec. 3.3). From (57), a_2 has the following expression

$$a_2 = \frac{1}{2a_1\phi_o}\left[\left(-\frac{2a_1^2 S_o^2}{\phi_o''^2}\sqrt{2G_c\,\ell_f}\hat{k}_o\right)^{2/3} + 2a_1(a_1 - 2)\phi_o - \frac{a_1^2 S_o^2}{\phi_o''} + \frac{2G_c}{\ell_f}\right]. \tag{58}$$

3. The coefficient a_3 multiplies the third-order term in the polynomial (4), thus it mainly influences states where damage is large. In [38], indeed, a_3 was related to the displacement jump $\tilde{w}$ at complete fracture of the specimen through the formula

$$a_3 = \frac{1}{a_2}\left[\frac{1}{2}\left(\frac{\tilde{w}S_o}{2G_c}\right)^2 - (1 + a_2)\right]. \tag{59}$$

Since this relation was derived within the context of linear elasticity, it cannot be straightforwardly extended to the finite strain case. Accordingly, it is just used to obtain an estimate of the parameter a_3. For damage occurring at small strains, formula (59) provides the exact value to assign to a_3 in order for the fracture jump to be $\tilde{w}$. On the contrary, for damage onset at large strains it gives only an approximate value. Further indications are given by the drawing of the cohesive curve, as discussed in the following.

To better highlight the role of the different cohesive parameters we now consider two different forms of the Ogden elastic strain energy density with different elastic parameters: one with $N = 1$ in the series $(25)_3$ and $\mu_1 = 2.2$ MPa, $\alpha_1 = 2$, that we call quadratic energy ϕ_A, the other with $N = 2$

and $\{\mu_1, \mu_2\} = \{4.8, 0.01\}$ Mpa and $\{\alpha_1, \alpha_2\} = \{1.2, 5.1\}$, say ϕ_B. As shown in Fig. 1, such a choice of the elastic coefficients represents two plausible elastic response of a rubbery material, the former has a linear Piola stress at large stretches, whereas the latter shows the stress hardening at large stretches typical of elastomers.
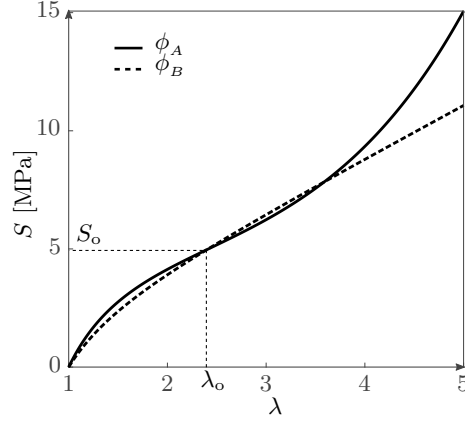

Figure 1: Piola stress S versus (elastic) stretch λ for the two strain energies ϕ_A and ϕ_B.

The cohesive curves $S = S(w)$ corresponding to these elastic energies are shown in Fig. 2 for $\ell_f = 5$ mm and different values of the parameters G_c, $\hat{k}_o$ and a_3. For a given G_c, the values of $\hat{k}_o$ and $\tilde{w}$ are assigned by supposing that the cohesive law is linear with the fracture opening $S = -\frac{S_o^2}{2G_c}w + S_o$, an expression which is the simplest triangular cohesive curve. Accordingly, $\hat{k}_o = -\frac{S_o^2}{2G_c}$ and $\tilde{w} = \frac{2G_c}{S_o}$. The coefficients a_1, a_2 and a_3 are derived from (56), (58) and (59). For low values of G_c, the cohesive curves recover the linear law when the energy density ϕ_A is used, whereas they deviate from linearity as G_c is increased. When the two terms energy density ϕ_B is considered, linearity is lost, as shown by the dashed curves of Fig. 2(a). In this case, the curves exhibit snap-back branches that are more pronounced for increasing values of G_c. The presence of a snap-back tail, indicated with a star in the figure, depends on the specific shape of ϕ_B, that has a convex branch where stiffness grows as stretches increase (see Fig. 1). This determines the fracture properties of the material. Indeed the softening process of fracture interrupts when the snap-back branch is encountered, and the catastrophic fracture leads to the final rupture of the specimen. As a consequence the recovery in the elastic stiffness for large stretches induces a brittle response

in the final stage of the fracture evolution.

A way to reduce the snap-back tails in the cohesive curves is to increase the initial slope $\hat{k}_\mathrm{o}$. This is shown in Fig. 2(b). Starting from the solid-line curve obtained by considering the strain energy density ϕ_B, and assigning $G_c = 60$ MPa mm, $\hat{k}_\mathrm{o} = -0.2058$ MPa/mm and $a_3 = -0.6851$, i.e., the dashed curve $G_c = 60$ MPa mm of Fig. 2(a), the other curves are drawn by magnifying the initial slope by a factor of 2.5 and 10 (dashed-lines).

The influence of a_3 is also investigated. The dotted-line curves, are obtained by just varying the coefficient $a_3 < 0$, but keeping fixed $G_c = 60$ MPa mm and the initial slope of $10\hat{k}_\mathrm{o}$. The coefficient a_3 influences the final part of the cohesive curves. Large negative values of a_3 raise the curve tail, thus reduce the snap-back up to completely eliminate it. It turns out that the final catastrophic fracture is replaced by a recovery of stiffness that allows the material to further bear stresses.
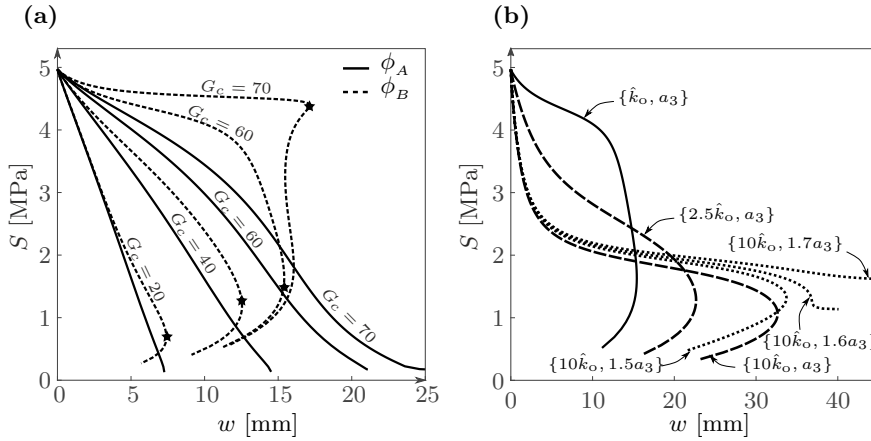
Figure 2: Cohesive curves for different values of the parameters G_c, $\hat{k}_\mathrm{o}$ and a_3. (a) curves for different values of G_c [MPa mm] in case of energy densities ϕ_A (solid-line) and ϕ_B (dashed-line); (b) starting from the solid-line curve, whose parameters are $G_c = 60$ MPa mm, $\hat{k}_\mathrm{o} = -0.2058$ MPa/mm, $a_3 = -0.6851$, other curves are drawn for different values of $\hat{k}_\mathrm{o}$ (dashed-line) and a_3 (dotted-line) with the elastic energy ϕ_B.

4 Numerical Examples

The variational model (23)-(24) was implemented in the finite element open-source framework FEniCS®[51].

The displacement and damage fields were projected over a piecewise affine finite element space (Lagrange elements) by using the same mesh domain. As the energy functional $\mathcal{I}$ defined in (6) for the general formulation and in (33) for the simple tension incremental problem is separately convex in each variable, an alternate minimization algorithm in the variables u and d was implemented. At a given time step, the solution of the iterative evolution of Sec. 3.2 was achieved iterating on the following subproblems until convergence:

1. The minimization of $\mathcal{I}$ with respect to u at fixed d is an unconstrained optimization problem solved as a nonlinear elastic problem with the prescribed boundary conditions through the Newton-Raphson method;

2. The minimization of $\mathcal{I}$ with respect to d at fixed u is a unilateral constrained quadratic optimization problem, which was solved through TAO (Tool-kit for Advanced Optimization).

Further details on the numerical implementation can be found in [47]. Simulations on both 1D or 2D geometries were carried out, although the results shown in the paper refer to the latter.

Two numerical examples are discussed in the following. As a first benchmark problem, we consider a rectangular test specimen subjected to tensile loadings. This example has twofold purpose: assessing the sensitivity of the model with respect to the different constitutive parameters and demonstrating the ability of the proposed modelling framework of capturing the large-strain behaviour of double network elastomers. Afterwards, we use a double edge notched specimen in tension to validate the model prediction up to the specimen rupture.

The rectangular specimen used to carry out the sensitivity analysis is shown in Fig. 3 together with the boundary conditions and the mesh. This latter was made up of 12.000 Lagrange triangular elements. The height of the specimen was kept fixed at 4 mm, whereas three different lengths were considered $\ell = \{6, 13, 20\}$ mm as discussed in the following. In all simulations two different sets of elastic parameters were used to assess the effects of the particular form of the Ogden energy on the fracture properties of the material, that correspond to the energies ϕ_A and ϕ_B in Fig. 1; the other constitutive parameters are the ones in Tab. 1 except where stated.
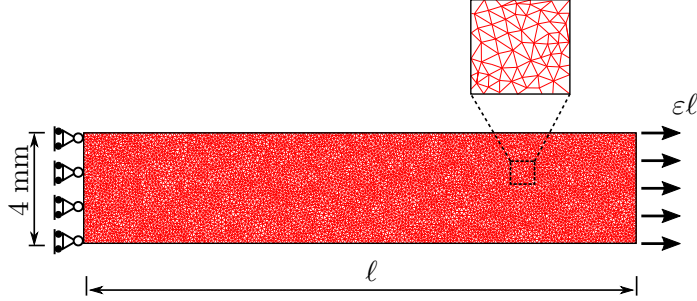
Figure 3: Geometry of the rectangular specimen with details of the mesh made of about 12.000 Lagrange triangular elements. The height of the specimen was kept fixed in all numerical tests, whereas different lengths $\ell = \{6, 13, 20\}$ mm were considered.

Table 1: Constitutive parameters used in the numerical examples.

Elastic		
ϕ_A:	$\mu_1 = 2.2$ MPa	$\alpha_1 = 2$
ϕ_B:	$\{\mu_1, \mu_2\} = \{4.8, 0.01\}$ MPa	$\{\alpha_1, \alpha_2\} = \{1.2, 5.1\}$
Fracture		
$\ell_{\mathrm{f}} = 5$ mm, $\quad G_c = 60$ MPa mm, $\quad \lambda_{\mathrm{o}} = 2.4, \quad \hat{k}_{\mathrm{o}} = -0.21$ MPa/mm, $\quad \tilde{w} = 24.15$ mm		

We point out that the coefficients a_1, a_2 and a_3 were obtained from G_c, $\hat{k}_{\mathrm{o}}$ and $\tilde{w}$ by using the formulas (56), (58) and (59).

The Piola stress S in terms of overall strain ε as well as the damage profiles along the mean axis of the bar are plotted in Figs. 4 and 5 for the two energy densities ϕ_A and ϕ_B and different values of the energy release rate G_c.

By increasing values of G_c, the maximum strain attained at rupture grows with a larger region in which a pseudo-ductile response is achieved. With the energy ϕ_A, the response with $G_c = 20$ MPa mm (green curve in Fig. 4) shows a sudden drop in the stress caused by an abrupt damage growth at the end of the elastic stage, that almost immediately reaches values close to 1 as shown by the green damage profiles in the figure. The resulting overall behaviour is brittle. For larger values of G_c, the drop in the stress is smoothed out with cohesive-like softening curves; in terms of damage this behaviour is produced by the phase field variable progressively growing and enlarging.
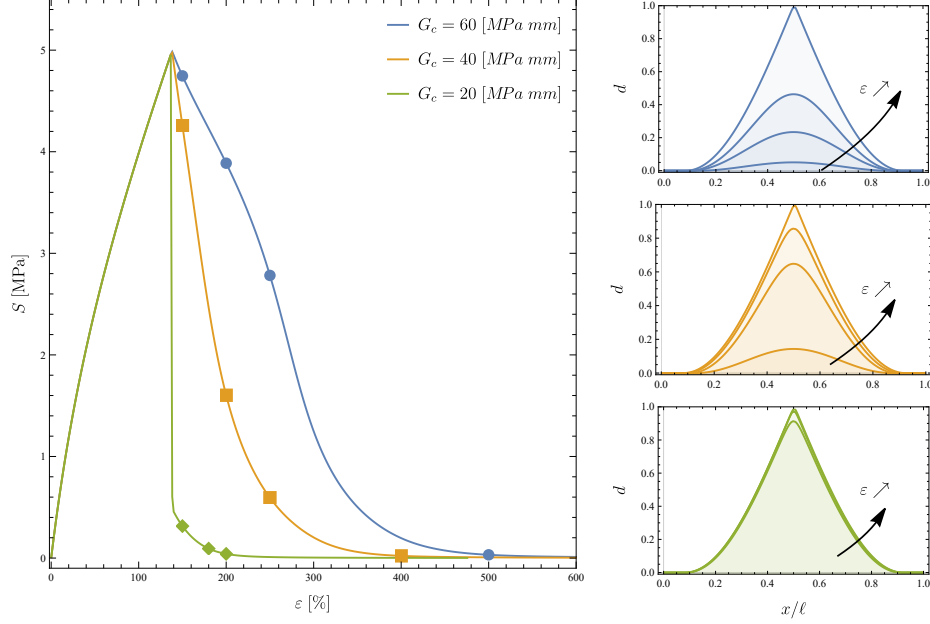
29

Figure 4: Influence of the energy release rate G_c in the case of elastic energy ϕ_A. Piola stress S versus overall strain ε for $G_c = \{20, 40, 60\}$ MPa mm. The insets show the damage profiles d evaluated on the mean axis of the bar at the different stretch levels indicated on each curve.

For the elastic coefficients in the energy ϕ_B, brittle and cohesive responses are obtained for $G_c = 20$ and 40 MPa mm, respectively. For $G_c = 60$ MPa mm, the specimen exhibits a pseudo-ductile behaviour in which two response stages are clearly observed: a softening branch with a low slope, followed by a sudden drop in the stress. As the damage profiles show, in the first stage of moderate softening, the damage grows slowly whilst expanding trough the bar. At the end of this phase, the damage has covered the entire domain and has reached its maximum value of 0.3. Thereafter damage immediately increases producing the rupture of the specimen with the resulting stress rapidly decreasing to zero.

Since the gradient term in the fracture energy make the model size dependent, the effect of specimen length is analysed in Fig. 6 for $\ell = \{6, 13, 20\}$ mm. The results indicates that when ℓ is comparable with the internal length $\ell_{\rm f} = 5$ mm the response is cohesive, whereas sufficiently long bars displays a brittle or quasi-brittle failure for both the energies ϕ_A
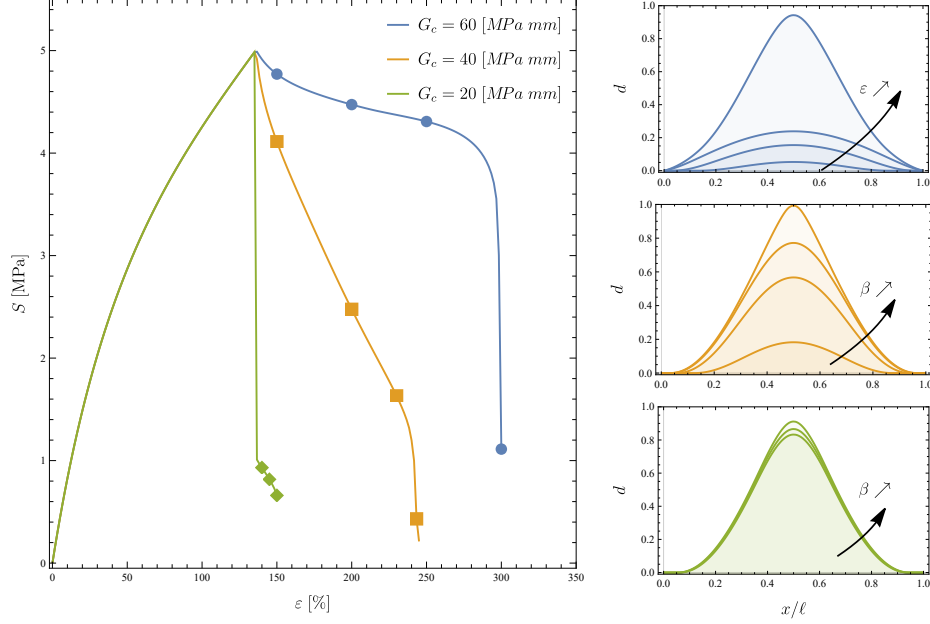
Figure 5: Influence of the energy release rate G_c in the case of elastic energy ϕ_B. Piola stress S versus overall strain ε for $G_c = \{20, 40, 60\}$ MPa mm. The insets show the damage profiles d evaluated on the mean axis of the bar at the different stretch levels indicated on each curve.

(Fig. 6a) and ϕ_B (Fig. 6b).

In Fig. 6, the dependency of the material response on the slope of the cohesive curve $\hat{k}_o$ is investigated. This constitutive parameter is directly related through Eq. (58) to a_2. As shown by the results, $\hat{k}_o$ controls the stress decrease at the damage onset, and it regulates the softening branch with moderate slope, that is associated to a process of damage propagation all over the domain and it may induce a snap-back of the softening curve, for sufficiently large value, resulting in a discontinuous stress drop. The simulations start with the value of $\hat{k}_o$ in Tab. 1 (blue curve in the figure), with a cohesive–like behaviour for both the energies ϕ_A (Fig. 7a) and ϕ_B (Fig. 7b).

Finally, the influence of coefficient a_3 is analysed in Fig. 8. We start from the green curve in Fig. 7(b), that corresponds to $\hat{k}_o = -2$ MPa/mm and we increase the value of a_3 by a factor of 2 and 4, respectively, such that $a_3 = \{-0.68, -1.36, -2.72\}$. As pointed out in Sec. 3.5, increasing

values of a_3 lead to a recovery of the material stiffness, with a consequent transition from a softening (green curve) to a hardening response (orange and blue curves). In all cases, it is seen a significant stress drop at the end of the elastic phase, that corresponds to the sudden occurrence of a localized damage in the central part of the specimen, with the phase field variable reaching 0.2. Thereafter different damage evolution regimes are seen: for the blue curve ($a_3 = -0.68$) the damage increases sharply in the central part of the specimen until it reaches the value of 1 meaning that the specimen is completely broken; on the contrary, the blue curve shows a rather limited increase in the damage intensity, that stays below 0.4, but the support of the phase field variable enlarges, up to the point where it occupies the entire bar. This type of evolution resembles a sort of "plastic-wave" that propagates inside the bar (damage-wave in this case) and has indeed been observed in double-network elastomers.

As a general remark for the model behaviour, in all simulations it was observed that the rate of damage growth is proportional to the slope of the softening branch. Furthermore, a broadening of the damage localization zone is observed when the softening branch is convex, whereas a concave softening branch produces damage localization is narrow regions.
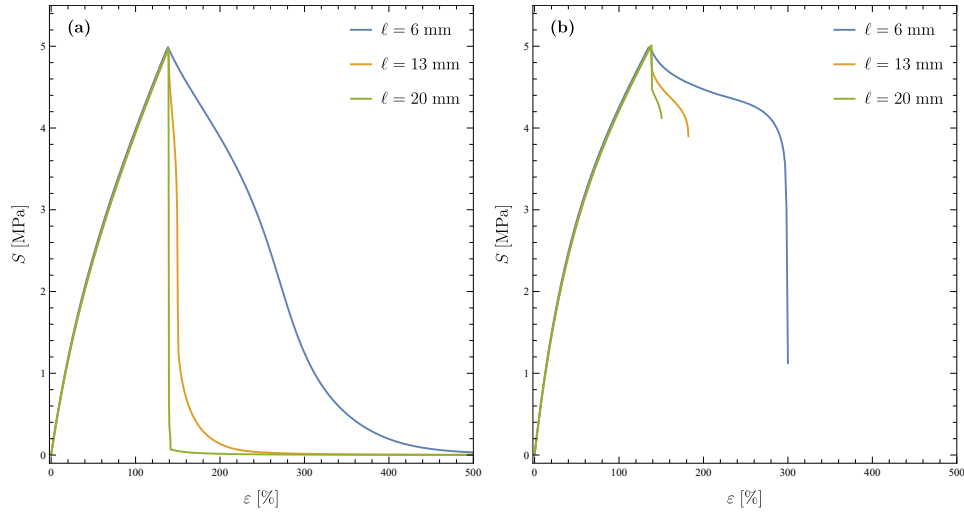

Figure 6: Size dependency of the model. Piola stress vs. strain curves for different bar lengths $\ell = \{6, 13, 20\}$ mm and elastic energies ϕ_A (a) and ϕ_B (b).

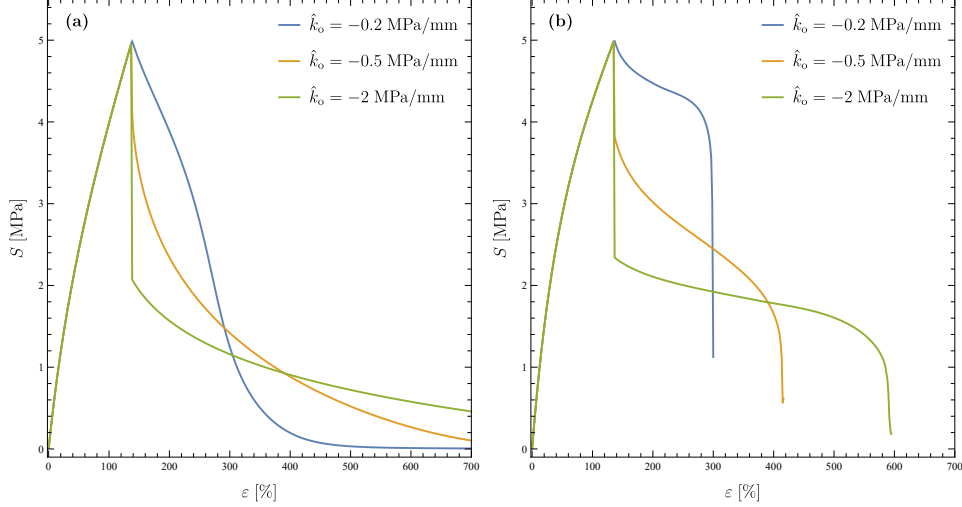Having shown the main features of the proposed model, we are now in

Figure 7: Influence of the cohesive parameters $\hat{k}_{\rm o}$. Piola stress vs. strain for different values of the cohesive curve slope $\hat{k}_{\rm o} = \{-0.2, -0.5, -2\}$ MPa/mm and elastic energies ϕ_A (a) and ϕ_B (b).

the position of comparing the model prediction against the experimental data on double network elastomers. The experiments used to calibrate the model are the ones reported in [35], where a cross-linked elastomer was first swollen in monomer and subsequently polymerized to create the so-called double network. This novel class of elastomers displays unique mechanical features due to the combined use of a stretchy elastomeric matrix with a stiff filler network, that make the failure of the elastomer pseudo-ductile at large strain.

The peculiarities of the experimental response are readily seen from the data in Fig. 9 where the Piola stress, S, is plotted against the normalized displacement at bar's end, ε. The initial part of the curve resembles the typical response of an elastomeric material with a pronounced nonlinear elastic behaviour. The elastic phase terminates at about $\varepsilon = 1.4$ where a sharp decrease in the stress appears. Microscopically this drop corresponds to the emergence of a very localized damage region. By continuing loading, the applied force remains constant and the stress-strain plot shows a plateau for a wide range of stretches. The formation of a neck and its propagation along the specimen is observed in this region. When necking has expanded all over the sample, at about $\varepsilon = 4.2$, the damage start increasing uniformly, yet the overall stiffness of the sample grows. This behaviour is a competition
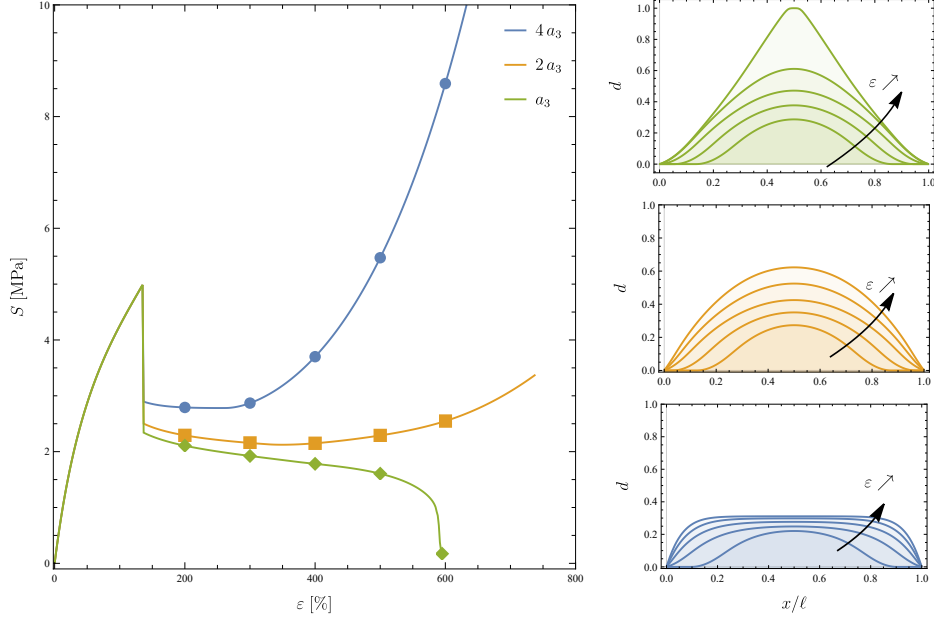
Figure 8: Influence of the fracture parameter a_3. Piola stress vs. strain for $a_3 = \{-0.68, -1.36, -2.72\}$ with the elastic parameters in ϕ_B. The insets show the damage profile at the different strain levels indicated in the figure.

between the stress softening induced by the damage and the stiffening caused by the intact polymer chains being almost completely stretched. Such a peculiar behaviour for an elastomer was reported for the first time in [35].

Remarkably the proposed model is able to capture the main features seen in the experimental data as the fitting in Fig. 9 proves. The stress-strain plot displays three different curves along with the experimental points represented by open orange circles: the continuous orange curve, is the output of the model and has all the main characteristics of the experimental response, including the initial nonlinear elastic regime, the stress peak with the subsequent stress plateau and the stiffness increase at large strain. The green and orange dashed curves are indeed the elastic stresses of each of the two terms in the Ogden model (28) with the parameters $\{\mu_1, \alpha_1, \mu_2, \alpha_2\}$ in Tab. 2: at each material point, the elastic stress is the superposition of the response of two nonlinear springs, one with $\{\mu_1, \alpha_1\} = \{4.6 \text{ MPa}, 1.2\}$, that controls the response at low strains (dashed orange curve), and the other with $\{\mu_2, \alpha_2\} = \{0.012 \text{ MPa}, 5.5\}$ is activated at high strain and is

34

Table 2: Constitutive parameters used for the fitting of the experimental data in Fig. 9.

Elastic				
	$\{\mu_1, \mu_2\} = \{4.6, 0.012\}$ MPa	$\{\alpha_1, \alpha_2\} = \{1.2, 5.5\}$		
Fracture				
	$\ell_\mathrm{f} = 5$ mm,	$G_c = 100$ MPa mm,	$\lambda_\mathrm{o} = 2.4$,	$\hat{k}_\mathrm{o} = -0.37$ MPa/mm,	$a_3 = -4.73$

responsible for the strain hardening seen in the experiments (dashed green curve). In this sense the model resembles the microscopical model proposed in [52] where a two-phase material model was considered. The insets in Fig. 9 shows the damage field obtained from the numerical simulations at different level of strains. At the position designated with (a) in Fig. 9, the sudden appearance of a localized damage produces the drop in the stress seen in the experiments, that corresponds to the occurrence of a necked region in the central part of the specimen, as shown in Fig. 10. The corresponding strain level $\varepsilon = 1.4$ is used to calibrate the value of the parameter λ_o. At increasing level of strains, the necking enlarges with constant maximum value up to the stretch at which it has filled the whole specimen (region (b) in the figure). Thereafter (region (c)) the damage value starts increasing and at $\varepsilon = 4.55$ was $d = 0.33$. The hardening behaviour is achieved in the model by taking the absolute value of a_3 to be large enough ($a_3 = -4.73$ in this case).

The final benchmark corresponds to the deformation of a double notch tension specimen that is normally used to estimate the critical fracture energy (see for instance [25, 45]). The dimensions of the specimen, boundary conditions and mesh for this configuration are displayed in Fig. 11a. The constitutive parameters used in the simulation are those in Tab. 1 with the elastic energy ϕ_B, except for the fracture parameters $a_1 = 5.49$, $a_2 = -1.58$ and $a_3 = -0.54$. Figure 11b shows the stress-strain curves that displays typical brittle response expected from elastomers in this type of tests (see for instance the experiments in [53]). The numerical results show a very narrow cohesive region in which the damage rapidly propagates between the notches up to the point at which it occupies the entire width and immediately jumps to 1, leading to the catastrophic failure of the specimen. The corresponding deformed configurations are shown in Fig. 12 at different levels of the overall strain. At $\varepsilon = 0.6186$ the specimen is completely broken and, in fact, the central part of the specimen has reached $d = 1$, with the lateral parts being almost unloaded.
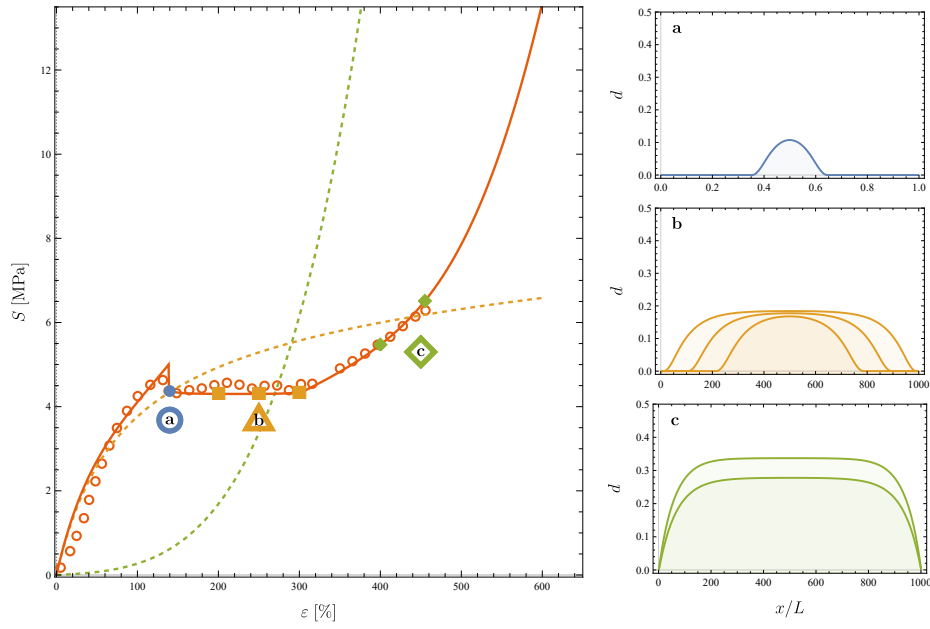
Figure 9: Piola stress S versus overall strain ε for a double network elastomers: open circles - experimental data from [35], orange continuous curve - model prediction, dashed curve - response of purely elastic model. The fitting is achieved with the model parameters in Tab. 2. The insets show the damage profile along the specimen middle axis at the strain levels (a), (b) and (c) indicated in the plot.
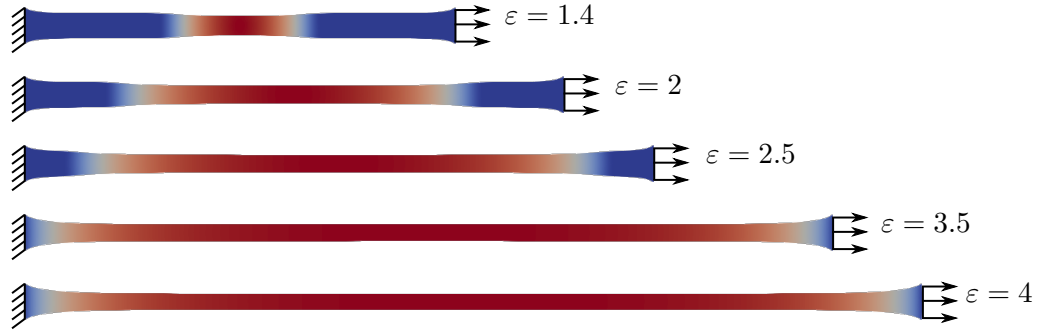
36

Figure 10: Deformed configuration of the rectangular specimen used for fitting the data in Fig. 9. The plateau in the stress-strain curves corresponds to the propagation of a necking region along the bar. The colormap represents the damage intensity, red being the damage with higher damage.
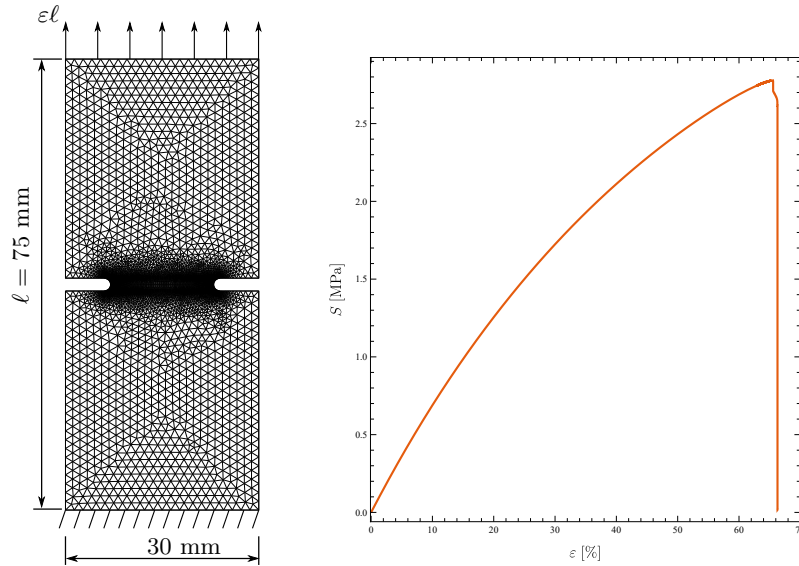

Figure 11: Geometry, mesh and boundary conditions of the double notch tensions specimen (left). Stress-strain curve for the constitutive parameters in Tab:1.
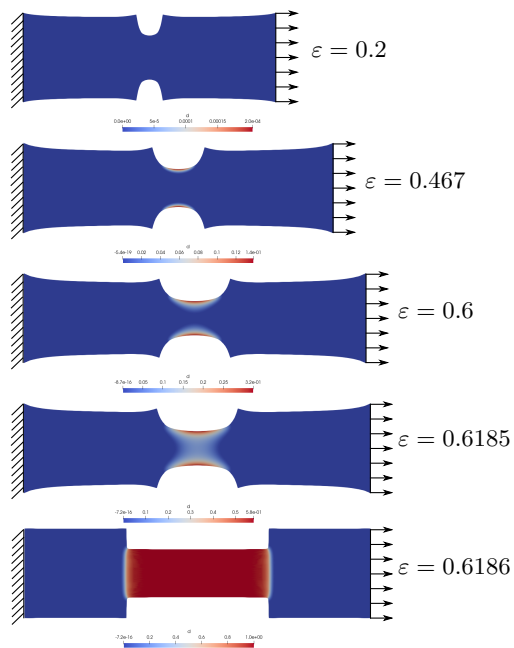
Figure 12: Deformed configuration of the double notch tension specimen used for the numerical experiment in Fig. 11. The colormap displays the intensity of the damage field.

5 Conclusions

We have presented a novel phase-field model for the cohesive failure of elastomers at large strain. The elastic response of the model is described through an Ogden-like strain energy density, which has the advantage of accurately matching the quasi-static response of many materials up to significant strains. Fracture was incorporated by complementing the Ogden formulation with a phase-field variable, whose evolution was derived in a consistent thermodynamic framework by invoking the three principles of damage irreversibility, stability conditions and energy balance.

The fracture energy is defined in terms of 5 constitutive parameters: the energy release rate G_c, the internal length ℓ_f, that naturally arises from the gradient term in the energy, and 3 coefficients a_1, a_2 and a_3 that defines the energetic degradation function responsible of the stiffness decrease induced by damage. The solution of a one-dimensional problem of a bar under tension is used to calibrate the cohesive parameters and give them a clear physical meaning: a_1 is related to the stretch at the damage onset in the one-dimensional test, a_2 depends on the slope of the cohesive curve, which is normally considered a material property, and, finally, a_3 is put in relation to the displacement jump at complete specimen fracture. By properly tuning these constitutive parameters, the model is capable of describing a variety of fracture modes including brittle and pseudo-ductile failures, whereas most of the phase field models at large strain currently available in the literature can only describe brittle fracture. As such, the model is applicable to a broad class of materials, not only rubber or elastomeric composites, but also biological tissues. In this work, it was applied to double-network elastomers, by reproducing the pseudo-ductile failure that they experience in simple tension tests. The model has accurately captured the peculiar features of the fracture process, such as the necking propagation, and the hardening stage at large strains.

The derivation of the modelling equations was carried out by the perfect incompressibility of the matrix, as usually assumed for rubber. However, experimental evidence shows that fracture may occur due to the coalescence of voids and the subsequent propagation of the defects, that may lead to a reduction of the apparent bulk modulus. Therefore, further development of the model include the possibility of degrading with the phase-field variable both volumetric and isochoric parts of the energy. In addition, since viscous effects may become significant during the propagation of fractures, the incorporation of viscoelastic effects appears of paramount importance to correctly describe the dynamic evolution of fracture in elastomeric compounds.

Acknowledgement

References

[1] R. W. Ogden, Compressible Rubberlike Solids Large deformation isotropic elasticity : on the correlation of theory and experiment for compressible rubberlike solids, Proceedings of the Royal Society A: Mathematical, Physical and Engineering Sciences 328 (1575) (1972) 567–583.

[2] R. W. Ogden, Large deformation isotropic elasticity – on the correlation of theory and experiment for incompressible rubberlike solids, Proceedings of the Royal Society of London. A. Mathematical and Physical Sciences 326 (1567) (1972) 565–584. `doi:10.1098/rspa.1972.0026`.

[3] J. C. Simo, R. L. Taylor, Quasi-incompressible finite elasticity in principal stretches. continuum basis and numerical algorithms, Computer Methods in Applied Mechanics and Engineering 85 (1991) 273–310. `doi:10.1016/0045-7825(91)90100-K`.

[4] O. H. Yeoh, On the Ogden strain-energy function, Rubber Chemistry and Technology 70 (2) (1997) 175–182. `doi:10.5254/1.3538422`.

[5] G. Saccomandi, Mechanics and Thermomechanics of Rubberlike Solids, cism lectu Edition, no. January, 2004. `doi:10.1007/978-3-7091-2540-3`.

[6] M. Destrade, G. Saccomandi, I. Sgura, Methodical fitting for mathematical models of rubber-like materials, Proceedings of the Royal Society A: Mathematical, Physical and Engineering Sciences 473 (2198) (2017). `arXiv:1608.05801`, `doi:10.1098/rspa.2016.0811`.

[7] V. Agostiniani, A. DeSimone, Ogden-type energies for nematic elastomers, International Journal of Non-Linear Mechanics 47 (2) (2012) 402–412. `doi:10.1016/j.ijnonlinmec.2011.10.001`.
URL `http://www.sciencedirect.com/science/article/pii/S0020746211002447`

[8] A. Goriely, L. A. Mihai, Liquid crystal elastomers wrinkling, Nonlinearity 34 (8) (2021) 5599–5629. `doi:10.1088/1361-6544/ac09c1`.

[9] N. J. Mills, C. Fitzgerald, A. Gilchrist, R. Verdejo, Polymer foams for personal protection: Cushions, shoes and helmets, Composites Science and Technology 63 (16) (2003) 2389–2400. `doi:10.1016/S0266-3538(03)00272-0`.

[10] J. Ciambella, A. Bezazi, G. Saccomandi, F. Scarpa, Nonlinear elasticity of auxetic open cell foams modeled as continuum solids, Journal of Applied Physics 117 (18) (2015) 184902. `doi:10.1063/1.4921101`.
URL `http://scitation.aip.org/content/aip/journal/jap/117/18/10.1063/1.4921101`

[11] R. Moran, J. H. Smith, J. J. García, Fitted hyperelastic parameters for Human brain tissue from reported tension, compression, and shear tests, Journal of Biomechanics 47 (15) (2014) 3762–3766. `doi:10.1016/j.jbiomech.2014.09.030`.
URL `http://dx.doi.org/10.1016/j.jbiomech.2014.09.030`

[12] D. B. Macmanus, B. Pierrat, J. G. Murphy, M. D. Gilchrist, Mechanical characterization of the P56 mouse brain under large-deformation dynamic indentation, Scientific Reports 6 (February) (2016) 1–9. `doi:10.1038/srep21569`.

[13] L. A. Mihai, S. Budday, G. A. Holzapfel, E. Kuhl, A. Goriely, A family of hyperelastic models for human brain tissue, Journal of the Mechanics and Physics of Solids 106 (2017) 60–79. `doi:10.1016/j.jmps.2017.05.015`.
URL `http://dx.doi.org/10.1016/j.jmps.2017.05.015`

[14] E. I. Saavedra Flores, S. Adhikari, M. I. Friswell, F. Scarpa, Hyperelastic finite element model for single wall carbon nanotubes in tension, Computational Materials Science 50 (3) (2011) 1083–1087. `doi:10.1016/j.commatsci.2010.11.005`.
URL `http://dx.doi.org/10.1016/j.commatsci.2010.11.005`

[15] K. C. Valanis, The Valanis–Landel strain energy function Elasticity of incompressible and compressible rubber-like materials, International Journal of Solids and Structures 238 (September 2021) (2022) 111271. `doi:10.1016/j.ijsolstr.2021.111271`.
URL `https://doi.org/10.1016/j.ijsolstr.2021.111271`

[16] R. W. Ogden, G. Saccomandi, I. Sgura, Fitting hyperelastic models to experimental data, Computational Mechanics 34 (6) (2004) 484.

[17] G. A. Francfort, J. J. Marigo, Revisiting brittle fracture as an energy minimization problem, Journal of the Mechanics and Physics of Solids 46 (8) (1998) 1319–1342. `doi:10.1016/S0022-5096(98)00034-9`.

[18] B. Bourdin, G. A. Francfort, J. J. Marigo, Numerical experiments in revisited brittle fracture, Journal of the Mechanics and Physics of Solids 48 (4) (2000) 797–826. `doi:10.1016/S0022-5096(99)00028-9`.

[19] B. Bourdin, G. A. Francfort, J. J. Marigo, The variational approach to fracture, 2008. `doi:10.1007/978-1-4020-6395-4`.

[20] C. Miehe, M. Hofacker, F. Welschinger, A phase field model for rate-independent crack propagation: Robust algorithmic implementation based on operator splits, Computer Methods in Applied Mechanics and Engineering 199 (45-48) (2010) 2765–2778. `doi:10.1016/j.cma.2010.04.011`.
URL `http://dx.doi.org/10.1016/j.cma.2010.04.011`

[21] K. Pham, H. Amor, J. J. Marigo, C. Maurini, Gradient damage models and their use to approximate brittle fracture, International Journal of Damage Mechanics 20 (4) (2011) 618–652. `doi:10.1177/1056789510386852`.

[22] C. Miehe, L. M. Schänzel, Phase field modeling of fracture in rubbery polymers. Part I: Finite elasticity coupled with brittle failure, Journal of the Mechanics and Physics of Solids 65 (1) (2014) 93–113. `doi:10.1016/j.jmps.2013.06.007`.
URL `http://dx.doi.org/10.1016/j.jmps.2013.06.007`

[23] J. J. Marigo, C. Maurini, K. Pham, An overview of the modelling of fracture by gradient damage models, Meccanica 51 (12) (2016) 3107–3128. `doi:10.1007/s11012-016-0538-4`.

[24] G. Del Piero, G. Lancioni, R. March, A variational model for fracture mechanics: Numerical experiments, Journal of the Mechanics and Physics of Solids 55 (12) (2007) 2513–2537. `doi:10.1016/j.jmps.2007.04.011`.

[25] P. J. Loew, B. Peters, L. A. Beex, Rate-dependent phase-field damage modeling of rubber and its experimental parameter identification,

Journal of the Mechanics and Physics of Solids 127 (2019) 266–294. doi:10.1016/j.jmps.2019.03.022.
URL https://doi.org/10.1016/j.jmps.2019.03.022

[26] C. Hesch, K. Weinberg, Thermodynamically consistent algorithms for a finite-deformation phase-field approach to fracture, International Journal for Numerical Methods in Engineering 99 (12) (2014) 906–924. doi:10.1002/nme.4709.
URL http://onlinelibrary.wiley.com/doi/10.1002/nme.3279/fullhttps://onlinelibrary.wiley.com/doi/10.1002/nme.4709

[27] D. Henao, C. Mora-Corral, X. Xu, A numerical study of void coalescence and fracture in nonlinear elasticity, Computer Methods in Applied Mechanics and Engineering 303 (2016) 163–184. doi:10.1016/j.cma.2016.01.012.
URL http://dx.doi.org/10.1016/j.cma.2016.01.012

[28] A. Kumar, G. A. Francfort, O. Lopez-Pamies, Fracture and healing of elastomers: A phase-transition theory and numerical implementation, Journal of the Mechanics and Physics of Solids 112 (2018) 523–551. doi:10.1016/j.jmps.2018.01.003.
URL https://doi.org/10.1016/j.jmps.2018.01.003

[29] A. Kumar, O. Lopez-Pamies, The phase-field approach to self-healable fracture of elastomers: A model accounting for fracture nucleation at large, with application to a class of conspicuous experiments, Theoretical and Applied Fracture Mechanics 107 (February) (2020) 102550. doi:10.1016/j.tafmec.2020.102550.
URL https://doi.org/10.1016/j.tafmec.2020.102550

[30] X. Poulain, V. Lefèvre, O. Lopez-Pamies, K. Ravi-Chandar, Damage in elastomers: nucleation and growth of cavities, micro-cracks, and macro-cracks, International Journal of Fracture 205 (1) (2017) 1–21. doi:10.1007/s10704-016-0176-9.

[31] X. Poulain, O. Lopez-Pamies, K. Ravi-Chandar, Damage in elastomers: Healing of internally nucleated cavities and micro-cracks, Soft Matter 14 (22) (2018) 4633–4640. doi:10.1039/c8sm00238j.

[32] B. Talamini, Y. Mao, L. Anand, Progressive damage and rupture in polymers, Journal of the Mechanics and Physics of Solids 111 (2018) 434–457. doi:10.1016/j.jmps.2017.11.013.

URL https://linkinghub.elsevier.com/retrieve/pii/S0022509617303939

[33] B. Li, N. Bouklas, A variational phase-field model for brittle fracture in polydisperse elastomer networks, International Journal of Solids and Structures 182-183 (2020) 193–204. `doi:10.1016/j.ijsolstr.2019.08.012`.
URL https://doi.org/10.1016/j.ijsolstr.2019.08.012

[34] P. A. Toulemonde, J. Diani, P. Gilormini, N. Desgardin, On the account of a cohesive interface for modeling the behavior until break of highly filled elastomers, Mechanics of Materials 93 (2016) 124–133. `doi:10.1016/j.mechmat.2015.09.014`.

[35] P. Millereau, E. Ducrot, J. M. Clough, M. E. Wiseman, H. R. Brown, R. P. Sijbesma, C. Creton, Mechanics of elastomeric molecular composites, Proceedings of the National Academy of Sciences of the United States of America 115 (37) (2018) 9110–9115. `doi:10.1073/pnas.1807750115`.

[36] L. Treloar, The Physics of Rubber Elasticity, Clarendon Press, Oxford, 2005.

[37] Z. Zhao, H. Lei, H. S. Chen, Q. Zhang, P. Wang, M. Lei, A multiscale tensile failure model for double network elastomer composites, Mechanics of Materials 163 (September) (2021) 104074. `doi:10.1016/j.mechmat.2021.104074`.
URL https://doi.org/10.1016/j.mechmat.2021.104074

[38] J. Y. Wu, A unified phase-field theory for the mechanics of damage and quasi-brittle failure, Journal of the Mechanics and Physics of Solids 103 (2017) 72–99. `doi:10.1016/j.jmps.2017.03.015`.
URL http://dx.doi.org/10.1016/j.jmps.2017.03.015

[39] J. J. Marigo, Constitutive relations in plasticity, damage and fracture mechanics based on a work property, Nuclear Engineering and Design 114 (3) (1989) 249–272. `doi:10.1016/0029-5493(89)90105-2`.

[40] G. Lancioni, Modeling the Response of Tensile Steel Bars by Means of Incremental Energy Minimization, Journal of Elasticity 121 (1) (2015) 25–54. `doi:10.1007/s10659-015-9515-8`.
URL http://dx.doi.org/10.1007/s10659-015-9515-8

[41] R. Alessi, J.-J. Marigo, S. Vidoli, Gradient damage models coupled with plasticity: variational formulation and main properties, Mechanics of Materials (jan 2014). `arXiv:s00205-014-0763-8`.
URL `http://www.sciencedirect.com/science/article/pii/S0167663614000039`

[42] G. Lancioni, R. Alessi, Modeling micro-cracking and failure in short fiber-reinforced composites, Journal of the Mechanics and Physics of Solids 137 (2020) 103854. `doi:10.1016/j.jmps.2019.103854`.
URL `https://doi.org/10.1016/j.jmps.2019.103854`

[43] J. Y. Wu, Robust numerical implementation of non-standard phase-field damage models for failure in solids, Computer Methods in Applied Mechanics and Engineering 340 (2018) 767–797. `doi:10.1016/j.cma.2018.06.007`.
URL `https://doi.org/10.1016/j.cma.2018.06.007`

[44] A. Mielke, T. Roubíček, Rate-independent systems, 2015.

[45] C. Miehe, F. Welschinger, M. Hofacker, Thermodynamically consistent phase-field models of fracture: Variational principles and multi-field FE implementations, International Journal for Numerical Methods in Engineering 83 (10) (2010) 1273–1311. `doi:10.1002/nme.2861`.
URL `http://onlinelibrary.wiley.com/doi/10.1002/nme.3279/full`

[46] R. W. Ogden, Nonlinear Elasticity. Theory and Applications, Cambridge University Press, Cambridge, 2001, Ch. 13, Pseudo, pp. 491–522.

[47] P. Farrell, C. Maurini, Linear and nonlinear solvers for variational phase-field models of brittle fracture, International Journal for Numerical Methods in Engineering 109 (5) (2017) 648–667. `arXiv:1511.08463, doi:10.1002/nme.5300`.

[48] G. Lancioni, V. Corinaldesi, Variational modelling of diffused and localized damage with applications to fiber-reinforced concretes, Meccanica 53 (3) (2018) 531–551. `doi:10.1007/s11012-017-0709-y`.
URL `https://idp.springer.com/authorize/casa?redirect_uri=https://link.springer.com/article/10.1007/s11012-017-0709-y&casa_token=ZOo19W15CUcAAAAA:YP1TokEOcd3w7O6JQcqafZYQpBNMhqeuzb2xgai-AqoqGQOR3qjJpROEhWL45M23183wN1hAuvs05OXdV`

[49] C. Nonato Da Silva, J. Ciambella, J. Barros, I. Costa, Analytical bond model for general type of reinforcements of finite embedment length in cracked cement based materials, International Journal of Solids and Structures 167 (2019) 36–47. `doi:10.1016/j.ijsolstr.2019.02.018`. URL `https://doi.org/10.1016/j.ijsolstr.2019.02.018https://linkinghub.elsevier.com/retrieve/pii/S002076831930099X`

[50] C. N. Da Silva, J. Ciambella, J. Barros, T. dos Santos Valente, I. Costa, A multiscale model for optimizing the flexural capacity of FRC structural elements, Composites Part B: Engineering 200 (2020) 108325. `doi:10.1016/j.compositesb.2020.108325`.

[51] A. Logg, K.-A. Mardal, G. Wells (Eds.), Automated Solution of Differential Equations by the Finite Element Method, Vol. 84 of Lecture Notes in Computational Science and Engineering, Springer Berlin Heidelberg, Berlin, Heidelberg, 2012. `doi:10.1007/978-3-642-23099-8`. URL `http://link.springer.com/10.1007/978-3-642-23099-8`

[52] D. De Tommasi, G. Puglisi, G. Saccomandi, Localized versus diffuse damage in amorphous materials, Physical Review Letters 100 (8) (2008) 1–4. `doi:10.1103/PhysRevLett.100.085502`.

[53] N. A. Hocine, M. N. Abdelaziz, A. Imad, Fracture problems of rubbers: J-integral estimation based upon η factors and an investigation on the strain energy density distribution as a local criterion, International Journal of Fracture 117 (1) (2002) 1–23. `doi:10.1023/A:1020967429222`.